Journal of Molecular Liquids 368 (2022) 120657

Contents lists available at ScienceDirect

Journal of Molecular Liquids

journal homepage: www.elsevier.com/locate/molliq

Removal of sulfonated azo Reactive Red 195 textile dye from liquid phase using surface-modified lychee (*Litchi chinensis*) peels with quaternary ammonium groups: Adsorption performance, regeneration, and mechanism

Venkata Subbaiah Munagapati [a], Hsin-Yu Wen [b], Anjani R.K. Gollakota [c], Jet-Chau Wen [a,c,*], Kun-Yi Andrew Lin [d], Chi-Min Shu [c], Guda Mallikarjuna Reddy [e], Grigory V. Zyryanov [e,f], Jhy-Horng Wen [g], Zhong Tian [h]

[a] Research Centre for Soil & Water Resources and Natural Disaster Prevention (SWAN), National Yunlin University of Science and Technology, Douliou, Yunlin 64002, Taiwan, ROC
[b] Department of Pathology, West China Hospital, Sichuan University, Chengdu 610041, PR China
[c] Department of Safety, Health, and Environmental Engineering, National Yunlin University of Science and Technology, Douliou, Yunlin 64002, Taiwan, ROC
[d] Department of Environmental Engineering, National Chung Hsing University, 250 Kuo-Kuang Road, Taichung, Taiwan, ROC
[e] Chemical Engineering Institute, Ural Federal University, 620002 Yekaterinburg, Russian Federation
[f] Ural Division of the Russian Academy of Sciences, I. Ya. Postovskiy Institute of Organic Synthesis, 22 S. Kovalevskoy Street, Yekaterinburg, Russian Federation
[g] Department of Electrical Engineering, Tunghai University, Taichung 40704, Taiwan, ROC
[h] State Key Laboratory of Hydraulics and Mountain River Engineering, Sichuan University, Chengdu, PR China

ARTICLE INFO

Article history:
Received 22 June 2022
Revised 14 October 2022
Accepted 19 October 2022
Available online 25 October 2022

Keywords:
Adsorption
G-LPP
Regeneration
Temperature
Reactive Red 195
Mechanism

ABSTRACT

In the present work, chemically modified lychee peels were synthesized using glycidyltrimethylammonium chloride (GTMAC) and used to remove Reactive Red 195 (RR 195) from an aquatic environment. Lychee peel powder (LPP), GTMAC-modified LPP (G-LPP), and RR-195/G-LPP were characterized by BET/BJH, FTIR, pH_{PZC}, XRD, and FE-SEM/EDX analyses. Adsorption tests were performed in batch mode, and various operational variables like initial dye concentration (25–250 mg/L), G-LPP mass (10–80 m g/30 mL), stirring speed (0–400 rpm), solution pH (1.0–10.0), contact time (0–480 min), and temperature (298–328 K) were studied to optimize the process. The solution pH strongly affects RR 195 removal efficiency. The maximal dye removal was 94.5%, achieved at pH 4.0. The non-linear assessment of isotherm and kinetics showed that the sorption system was fitted well by the Langmuir model (R^2 > 0.9899) and pseudo-first-order kinetic model (R^2 > 0.9918). The Langmuir maximum monolayer sorption capacities, q_{max}, at temperatures of 298, 308, 318, and 328 K are 144.9, 137.7, 130.1, and 124.2 mg/g, respectively, thus suggesting favorable adsorption at low temperatures. The E_a (activation energy) was computed to be 16.3 kJ/mol, which indicated that the adsorption behavior was mainly attributed to physisorption. The thermodynamic variables ΔH^o (−46.6 kJ/mol), ΔS^o (−133 J/mol K), and ΔG^o (−6.8693 ∼ −2.9777) revealed that the sorption process was exothermic, feasible, and spontaneous. The binding of RR 195 dye onto the G-LPP surface was through hydrogen bonding and electrostatic interactions. Desorption efficiency follows the order NaOH (91.2%) > NaCl (69.6%) > HCl (65.2%) > methanol (58.4%) > H_2SO_4 (48.1%) > acetone (45.5%) > ethanol (39.2%) > HNO_3 (31.6%). After five consecutive cycles of regeneration and reusability of G-LPP adsorption performance, the adsorption efficiency was better than 77.3%. The results show that G-LPP is a promising adsorbent for removing RR 195 dye from an aqueous solution.

1. Introduction

Worldwide industrialization is stunning. All the modern comforts enjoyed by mankind are a result of this rapid industrialization. However, the other facet of this modern lifestyle is also posing a toll on the environment. For example, the dyes released from various industries like textile, cosmetics, leather, food

* Corresponding author at: Research Centre for Soil & Water Resources and Natural Disaster Prevention (SWAN), National Yunlin University of Science and Technology, Douliou, Yunlin 64002, Taiwan, ROC.
E-mail address: wenjc@yuntech.edu.tw (J.-C. Wen).

https://doi.org/10.1016/j.molliq.2022.120657
0167-7322/

Nomenclature

A_T	equilibrium binding constant
B_T	Temkin constant
C_o and C_e	initial and equilibrium RR 195 solution concentrations
C_{Ae}	solid phase concentration at equilibrium
E_a	activation energy
k_1 and k_2	PFO and PSO rate constants
K_c	distribution constant
K_f	Freundlich constant
K_L	Langmuir constant
K	constant related to sorption energy
M	wight of G-LPP
n	Freundlich exponent
$1/n$	heterogeneity factor
q_e	adsorption uptake
$q_{e,\exp}$ and $q_{e,cal}$	experimental and calculated adsorption capacities
$q_{e1,cal}$ and q_{e2cal}	amount of dye adsorbed at equilibrium
q_t	adsorption uptake at time t
q_{max}	adsorption uptake
q_s	theoretical isotherm saturation uptake
R	universal gas constant (8.314 kJ/mol K)
t	time (min)
T	temperature (K)
V	volume of RR 195 solution (L)
α	initial adsorption rate
β	desorption constant
ε	Polanyi potential.

processing, and plastic are dangerous pollutants to the environment [1]. The key debilitating thing here is the nature of these dyes. They are recalcitrant, highly toxic, and dangerous synthetic dyes and pose a severe threat to humans by causing various cancers, and mutagenic events at the cellular and molecular levels [2]. In one of the reports, it was stated that the reactive dyes constitute 12% of the world's dye production as they possess excellent dyeing properties [3]. Reactive dyes are utilized in textile mills for their excellent wool, cellulose, and cotton fibers dyeing properties. About 20–40% of reactive dyes remain in the effluent after dyeing, making them highly colored and alkaline. Because of the –N = N- (azo) and $–SO_3H$ (sulphonate) groups, wastewater containing reactive dyes is very dangerous [4,5]. Therefore, the elimination of reactive dyes from the industrial effluents is the need of the hour. The current study was aimed at the removal of reactive mono azo dye RR 195 from the wastewater effluent.

Effective methods such as chemical coagulation-flocculation, ozonation, nano-filtration, micellar enhanced ultrafiltration, cloud point extraction, photocatalysis, ultrasound irradiation, membrane separation, advanced oxidation processes, and photodegradation [6,7] have been generally used for dye removal. Yet, these techniques have several downsides, including a high energy need, inadequate dye removal resulting in colorful effluent, the creation of by-products, a high operating cost, and sludge that may be more hazardous than the starting materials. As a result, it is critical to developing a more effective way for overcoming the restrictions on industrial wastewater effluents [7]. In this aspect, 'Adsorption' is a valuable process [8,9] due to its low initial cost, environmentally friendly, high efficiency, simple operation design, faster operation, and also does not produce secondary waste [10]. In the context of the elimination of dyes from industrial wastewater effluents, 'reducing the process cost', is the main objective for the researchers who are working in this domain. This objective is achievable through the use of 'non-economic, low-cost, widely available adsorbent materials, such as - industrial waste, and by-products (pulp, fertilizer, red mud, fly ash, etc.), agricultural wastes (seed, bark, shell, and peel of fruits, vegetables, etc.) and found in high amounts in nature organic–inorganic materials (algae, cellulose, fungi, resin, clay, etc.) [11,12]. However, these waste materials, may have low removal effectiveness, restricted surface area, inefficient regeneration, less active adsorption sites, and fewer surface functional groups [13], hence the need for modification with other materials.

The lychee is a tropical and subtropical fruiting tree native to Southeast Asia and Southern China. Scientifically it is also called *Litchi chinensis*, belonging to the *Sapindaceae* family. It was reported that the global lychee production is approximately 2.11 million tons which are currently being cultivated in many parts of the world [14]. The edible part of the fruit is the juicy flesh and its peel and seeds are usually discarded. It is estimated that 15% of the fresh lychee weight is its peel leading to the significant generation of lychee-related solid waste. It was also suggested that the lychee peel contains hydroxyl, amino, carbonyl, and carboxyl groups [15] hinting that lychee peel could be used as a sorbent in the elimination of dye ions from industrial wastewater effluents.

In recent years, various surface modification methods such as acid and base treatments [16,17], surfactants [18,19], etherification [20,21], esterification [22], impregnation [23], cationization [24,25], etc., have been suggested for anionic pollutant elimination. Surface modification principles are based on the carbonization of biomass or the insertion of functional groups or positively charged sites onto biosorbents [26]. Surface treatment using cationic polymers has shown to be the most effective of these approaches. Amines and quaternary ammonium reagents, like HDTMA (hexadecyltrimethylammonium), CTAB (cetyltrimethylammonium bromide), CHMAC (3-chloro-2-hydroxypropyl trimethylammonium chloride), GTMAC (glycidyltrimethylammonium chloride), PEI (polyethylenimine), and others can provide positively charged sites on the biosorbent. However, very hazardous cross-linking chemicals have been utilized in numerous research, and the modification procedure is sometimes rather complex.

In this investigation, a novel, easy, and less hazardous modification route for synthesizing quaternized lychee peel powder using GTMAC was developed and tested for RR 195 elimination from an aqueous environment. The impacts of different experimental parameters on the dye molecules' adsorption behavior were investigated. LPP, G-LPP, and RR-195/G-LPP were characterized by BET/BJH, XRD, FE-SEM/EDX, pH_{PZC}, and FTIR analysis. The characteristics like adsorption thermodynamics, isotherms, and kinetics were also determined using batch experimental methods. The reusability of the G-LPP was also evaluated by using the adsorption–desorption test. The mechanism for RR 195 adsorption onto G-LPP is also proposed.

2. Materials and methods

2.1. Materials and reagents

Lychee peels (LP) were collected at the local fruit market, Douliou, Taiwan. Reactive red 195 (MF: $C_{31}H_{19}ClN_7Na_5O_{19}S_6$; MW: 1136.31 g/mol), glycidyltrimethylammonium chloride (GTMAC),

sodium chloride (NaCl), sodium hydroxide (NaOH), acetic acid (CH_3COOH), sulfuric acid (H_2SO_4), and hydrochloric acid (HCl) were procured from Sigma-Aldrich (USA). All the chemicals were of AR grade without any additional purification. Fig. 1 depicts the chemical structure of RR 195 dye.

2.2. Preparation of RR 195 dye solution

By dissolving the correctly measured amount of dye in deionized (DI) water, a stock solution containing 1000 mg/L of dye was prepared. The solution for the adsorption studies was prepared by diluting the stock solution appropriately.

2.3. Preparation of G-LPP

The locally collected lychee peels were properly cleaned with DI water to remove the contaminants and dried under sunlight for 3–4 days. After that, LP was kept in an oven at 80 °C for 5 h to remove the residual moisture content. The dried peels were crushed and sieved to be a smaller particle by a 45 mesh sieve. The obtained powder was labeled as LPP.

The following steps were taken to modify the surface of LPP: In a 250 mL round bottomed flask, combine 1.0 g of LPP with 50 mL of NaOH (0.1% w/v) solution and 2.0 mL of GTMAC (0.0135 mol/g). The combined solution was then immersed in a water bath and constantly agitated at 60 °C for 3 h. Following completion, the obtained product was vigorously rinsed with DI water multiple times until the pH approached neutral and the supernatant turned clear. GTMAC modified-lychee peel powder (G-LPP) was formed by drying the cleaned product in an oven at 60 °C for 24 h. The G-LPP preparation method was presented in Fig. 2.

2.4. Surface characterization

The characteristics of the prepared samples (LPP, G-LPP, RR-195/G-LPP) were examined using various instrumental techniques. The surface morphologies and elemental content of the samples were determined using Field Emission-Scanning Electron Microscopy with an Energy Dispersive X-ray Spectrometer (FESEM-EDX; JSM-7610F plus; JEOL; Japan). Prior to analysis, the materials were first sputter coated with a homogeneous gold layer and then deposited onto a copper substrate. The surface area of samples (LPP and G-LPP) was calculated by Brunauer-Emmett-Teller (BET) technique via the low temperature multipoint N_2 adsorption–desorption isotherms (ASAP 2060; Micromeritics; USA). The samples were outgassed for 2 h at 100 °C before the analysis. Moreover, the pore-radius and pore-volume of the samples were calculated by the BJH (Barrett-Joyner-Halenda) technique. The functional groups of the surface of the samples were identified using Fourier Transform-Infrared Spectrometer (FT-IR; Thermo Nicolet iS10; USA). FTIR spectrum was recorded from 4000 to 400 cm^{-1} by accumulating at least 64 scans with a resolution of 4.0 cm^{-1} per sample. The samples were prepared using KBr (potassium bromide) disc method. The amorphous and crystalline nature of the samples (LPP and G-LPP) was determined by X-ray diffraction (XRD; Bruker AXS D8 Advance diffractometer; Germany) with CuKα (λ = 0.154 18 Å) radiation at 40 kV. The XRD patterns were acquired in the range $2\theta = 10 - 80°$ at a scanning rate of 2°/min.

The pH_{PZC} plays a vital role in determining the type of binding active site on the adsorbent. A point of zero charges is the pH value at which the charge sensed on the biosorbent surface becomes neutral. The pH_{PZC} is helpful for the evaluation of charges on the biosorbent surface [27]. The pH_{PZC} of the G-LPP was determined using the solid addition technique reported previously [28]. Firstly, 30 mL of (0.01 M) NaCl solution was transferred in a series of falcon tubes. The initial pH (pH_i) of each solution was adjusted in the range of 1.0–10.0 by using (0.1 M) HCl/NaOH solutions. Thereafter, 50 mg of G-LPP was added to each tube. The resultant solutions were stirred at room temperature at 200 rpm for 12 h until reaching equilibrium. After that, the solid was separated from the liquid phase and the final pH (pH_f) of each solution was measured using a pH-meter. The intersection point of the curves in the plot of ΔpH (pH_i - pH_f) against pH_i was taken as the pH_{PZC} of the G-LPP.

2.5. Batch adsorption experiments

Different adsorption properties, for instance, initial RR 195 dye concentration (25–250 mg/L), stirring speed (0–400 rpm), temper-

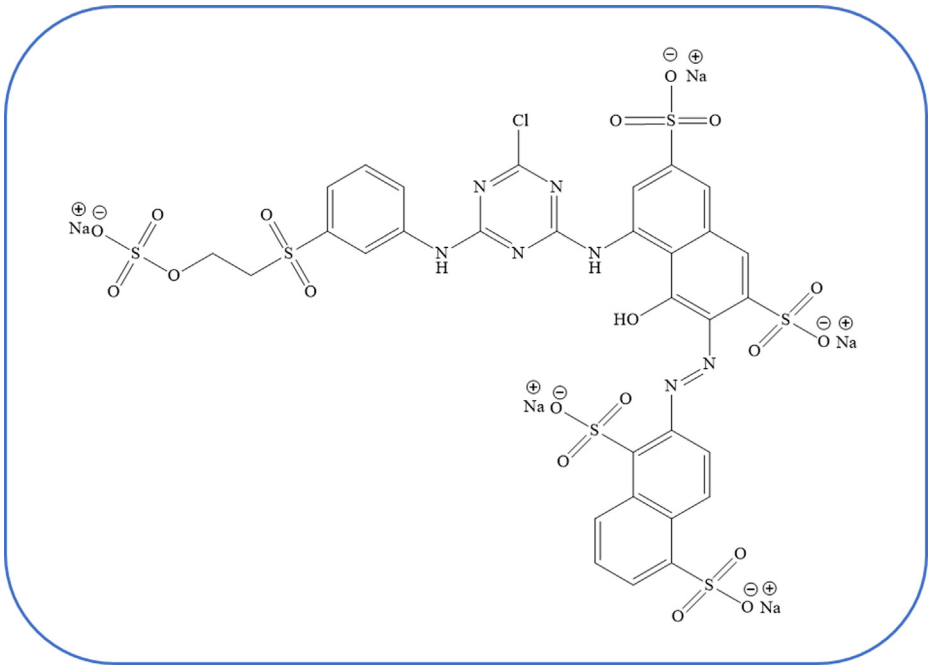

Fig. 1. Chemical structure of Reactive Red 195 dye.

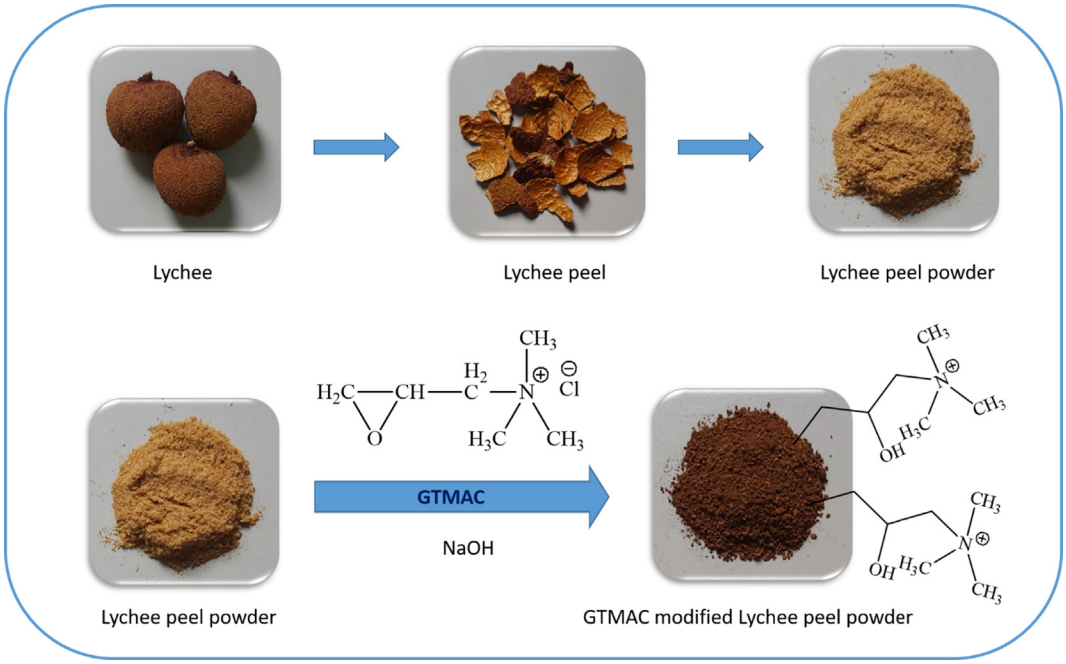

Fig. 2. The schematic representation of the G-LPP preparation.

ature (298–328 K), adsorbent dosage (10–80 mg), contact time (0–480 min), and pH (1.0–10.0) were investigated to determine their impact on the adsorption of RR 195 by G-LPP. The pH of the initial RR 195 dye solutions was adjusted by adding (0.1 M) HCl/NaOH, and the value was measured using a pH meter. The adsorption isotherms were conducted in various concentrations of RR 195 solutions ranging from 25 to 250 mg/L at different temperatures. Kinetic tests were conducted with an initial concentration of 25 ppm at multiple temperatures. Additionally, the effect of temperatures and the thermodynamic study was assessed in the 298–328 K range. All the batch biosorption tests were carried out with a series of 50 mL polypropylene centrifuge tubes containing a known concentration of RR 195 dye (30 mL) solution and a required amount of G-LPP. These mixtures were stirred in an electrical thermostatic reciprocating shaker during the desired contact time. The samples were withdrawn after a specified period of given intervals. All the samples were centrifuged at 8000 rpm for 5 min to separate the liquid from the solid and was analyzed for residual RR 195 using a UV–Visible spectrophotometer (JASCO V-750; Japan) at a maximum wavelength was 534 nm after proper dilutions. The temperatures (298, 308, 318, and 328 K) were maintained with an accuracy of ± 0.5 K. Each experiment was repeated under identical circumstances, and the results from the experiments were averaged, with error bars indicating standard deviation values. The adsorption uptake (q_e, *mg/g*) and removal efficiency (*R*, %) of RR 195 adsorbed on adsorbent is calculated by the following equations:

$$q_e = \frac{(C_o - C_e)\ V}{M} \tag{1}$$

$$R\% = \frac{C_o - C_e}{C_o} \times 100 \tag{2}$$

The best fitted isotherm model to the RR 195 sorption process onto G-LPP was determined using χ^2 (Chi-square) statistical error analysis. Significantly, the isotherm model that best reflects the adsorption process must have lower χ^2 values and higher regression correlation coefficient values (R^2). The following is the statistical error analysis equation for χ^2:

$$\chi^2 = \sum_{i=1}^{n} \frac{\left(q_{e,\ exp} - q_{e,\ cal}\right)^2}{q_{e,\ cal}} \tag{3}$$

2.6. Regeneration studies

To reveal the efficiency of G-LPP, the reusability was checked by completing numerous times adsorption/desorption cycles. The regeneration of RR 195 was performed using 0.1 M of NaOH, NaCl, HCl, H_2SO_4, HNO_3, and organic solvents (methanol, acetone, and ethanol), as the desorbing agents. The dried RR 195 dye-loaded G-LPP samples (50 mg) were maintained in a 50 mL polypropylene centrifuge tube (stirring at 200 rpm for 120 min) with the aforesaid desorbing eluents (30 mL). After the separation of the dye-loaded G-LPP from the solution by centrifugation, the concentration of RR 195 in the eluent was determined using a UV/Visible spectrophotometer. The standard deviations from the mean were represented by the error bars after each test was repeated in duplicate. After regeneration, the adsorbent was rinsed with DI water and then dried at 60 °C for 4 h. Then, it was reused for another adsorption/desorption cycle. The following equation considered percentage dye recovery:

$$Desorption\ (\%) = \frac{Conc.\ of\ dye\ desorbed\ by\ eluuent}{Conc.\ of\ dye\ adsorbed\ on\ adsorbent}\ X\ 100 \tag{4}$$

3. Results and discussion

3.1. Characterization (FT-IR, FE-SEM/EDX, BET/BJH, and XRD analysis)

FT-IR analyses were carried out to recognize the functional groups of the prepared sorbents such as LPP, G-LPP, and RR195 loaded G-LPP on its surface. FTIR spectra of LPP, G-LPP, and RR 195/G-LPP are portrayed in Fig. 3. In the spectrum of LPP (Fig. 3a), the broad and intense absorption peak at 3418 cm^{-1} corresponds to the O-H stretching vibration of carboxylic acids, phenols, and alcohols, as in cellulose, hemicellulose, pectin, and lignin, thus, showing the presence of free –OH groups on the LPP

surface [29]. The peak at 2917 cm^{-1} is attributed to the symmetric and asymmetric C-H stretching vibrations of aliphatic groups (–CH_3 or –CH_2) [30]. The peak observed at 2360 cm^{-1} is due to the C ≡ C stretching vibrations in alkyne groups [31]. The characteristic bands at 1749 and 1642 cm^{-1} indicate the stretching vibration of C = O from the carbonyl, carboxylic, or ester group [32]. The peak at 1540 cm^{-1} corresponds to the C = C vibrations from aromatic rings of lignin [33]. The peaks at 1421 and 1323 cm^{-1} correspond to the asymmetric stretching vibrations of the O-C-O group [34]. The bands at 1234 and 1058 cm^{-1} were assigned to the C-O stretching vibration of alcoholic groups and carboxylic acids [35]. The band at 1110 cm^{-1} was attributed to the C-O and C-O-C stretching vibrations in polysaccharides (cellulose, and hemicelluloses) [36]. In FTIR spectrum of G-LPP (Fig. 3b), characteristic bands around at 3418, 2917, 1749, 1642, 1540, 1421, 1323, 1110, and 1058 cm^{-1} were shifted to 3409, 2927, 1744, 1638, 1536, 1416, 1327, 1151, and 1079 cm^{-1}. The new peak was observed at 2130 cm^{-1}, verifying the presence of the quaternary ammonium group in G-LPP [37]. These changes indicate that the LPP surface has been successfully modified with GTMAC. After RR 195 dye adsorption (Fig. 3c), the absorption peak positions of G-LPP slightly shifted (3409, 2927, 1638, 1416, 1327, 1151, and 1079 cm^{-1} to 3422, 2912, 1616, 1412, 1332, 1155, and 1097 cm^{-1}), and two bands are disappeared (1744 and 1536 cm^{-1}). These changes show successful interactions of RR 195 dye molecules with the surface of G-LPP.

The surface texture and morphology of the LPP, G-LPP, and RR195/G-LPP samples were visualized by the FE-SEM analysis. The chemical characteristics of LPP, G-LPP, and RR195/G-LPP samples were identified by the EDX analysis. The FE-SEM/EDX images of LPP, G-LPP, and RR195/G-LPP are shown in Fig. 4. The morphology of the LPP (Fig. 4a) was irregular, smooth, non-porous, and homogeneous surface. The EDX spectrum revealed the presence of elements such as O, C, K, Ca, Mg, and Cl, on the LPP surface (Fig. 4b). After modification (Fig. 4c), the G-LPP surface was changed into a rough, uneven, irregular, heterogeneous, and porous texture. Generally, adsorbent surface roughness and porous texture play an essential role in dye adsorption performance because they provide a high internal surface area [9]. In the EDX spectrum of G-LPP (Fig. 4d), the major elements such as O, K, Ca, C, S, Na, and Cl have been identified on the G-LPP surface. After modification, the O, C, and Ca weight percentages were significantly increased and the K weight percentage is decreased. These elements with the higher composition in the G-LPP help to remove the RR 195 dye from the aqueous medium and it increases the adsorption efficiency of the G-LPP [38]. Those changes indicate that the LPP surface was successfully modified with GTMAC. After adsorption (Fig. 4e), the G-LPP surface is occupied by the RR 195 dye molecules and the surface became smoother, confirming the successful adsorption of RR 195 onto G-LPP. Another confirmation was made by EDX analysis which identifies the presence of the S (from the chemical structure of RR 195 dye) element on the G-LPP surface (Fig. 4f).

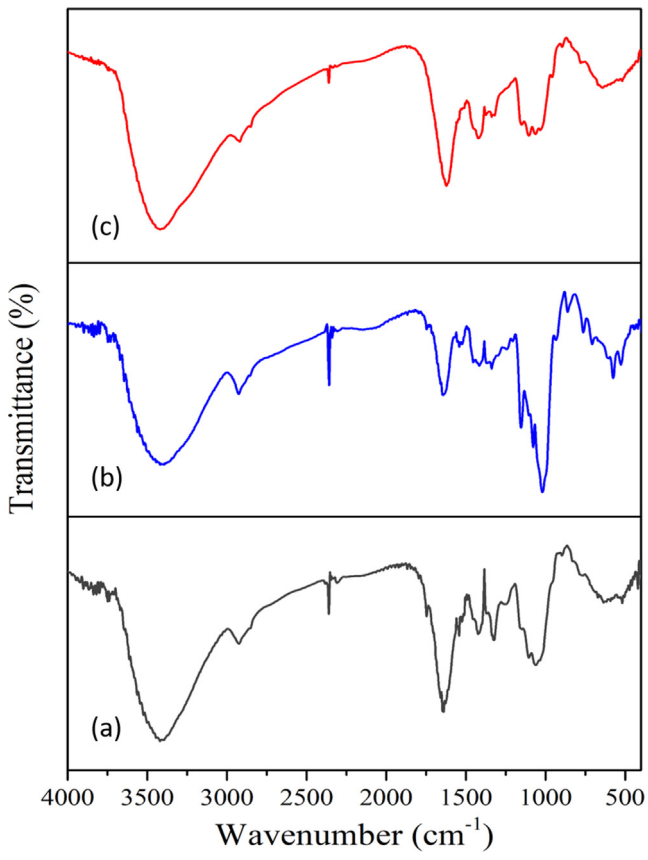

Fig. 3. FTIR spectra of LPP (a), G-LPP (b), and RR-195/G-LPP (C).

One of the most crucial parameters that regulate the adsorbent's adsorption effectiveness is the N_2 adsorption/desorption isotherm analysis. The surface area of LPP and G-LPP was calculated by BET, and the pore size distribution plots were derived by the BJH model. The surface areas of LPP and G-LPP were 2.813 and 17.48 m^2/g, respectively, with pore volumes of 0.0071 and 0.0358 cc/g and a pore radius of 1.537 and 2.293 nm. The surface area of LPP was increased significantly by almost 6.2 times after the modification, resulting in an increased number of sorption sites on the G-LPP surface for the RR 195 dye adsorption. According to IUPAC classifications, the LPP and G-LPP exhibited behavior of type-IV isotherm with an H_3-hysteresis at the higher relative pressures ($P/P_o > 0.4$) as depicted in Fig. 5(a,c), indicating that LPP and G-LPP have the mesoporous structure [39]. The pore size distributions for LPP and G-LPP as calculated by BJH were seen in Fig. 5(b, d). The pore size distribution of LPP and G-LPP was discovered to be in the range of 2.0–50 nm, indicating that the LPP and G-LPP are dominated majorly by mesoporous.

The XRD patterns of LPP and G-LPP are shown in Fig. 6. The XRD patterns of LLP (Fig. 6a) show the presence of a set of peaks at angular locations at 14.2°, 21.9°, and 32.1°. The characteristic peak of LPP at 14.2° was allocated to the crystalline peak of (1 1 0) for cellulose and those at 2θ = 21.9° and 32.1° were ascribed to the crystalline peaks of (0 0 2) and (0 0 4), respectively [40], which ascribed to the typical cellulose. After modification (Fig. 6b), the intensity of peaks decreased (2θ = 14.2° to 9.8° and 21.9° to 19.9°), and the peak at 32.1° was disappeared, which confirms the successful covered with GTMAC on the surface of LPP. The diffraction peak (2θ = 19.9°) in the XRD pattern of G-LPP represents the amorphous nature of the material.

3.2. Impact of pH

The pH solution is one of the most critical characteristics that influence adsorption since it influences solute solubility, ion concentration on the surface, adsorbent functional groups, and degree of ionization. Hence, the effect of pH on the adsorption of RR 195 by G-LPP was studied in the pH range of 1.0 to 10.0. As can be seen from Fig. 7a, with increased pH, the adsorption uptake (q_e) of G-LPP and removal rate (R) of RR 195 increased from 21.2 mg/g and 69% at pH 1.0 to 29.1 mg/g and 94.5% at pH 4.0, respectively. When the pH ranged from 4.0 to 10.0, the q_e and % decreased slowly. At pH < 4.0, the surface of G-LPP was presumably positively charged owing to the availability of a significant number of protons for the protonation of the –OH and –NH_2 groups of G-LPP hence the

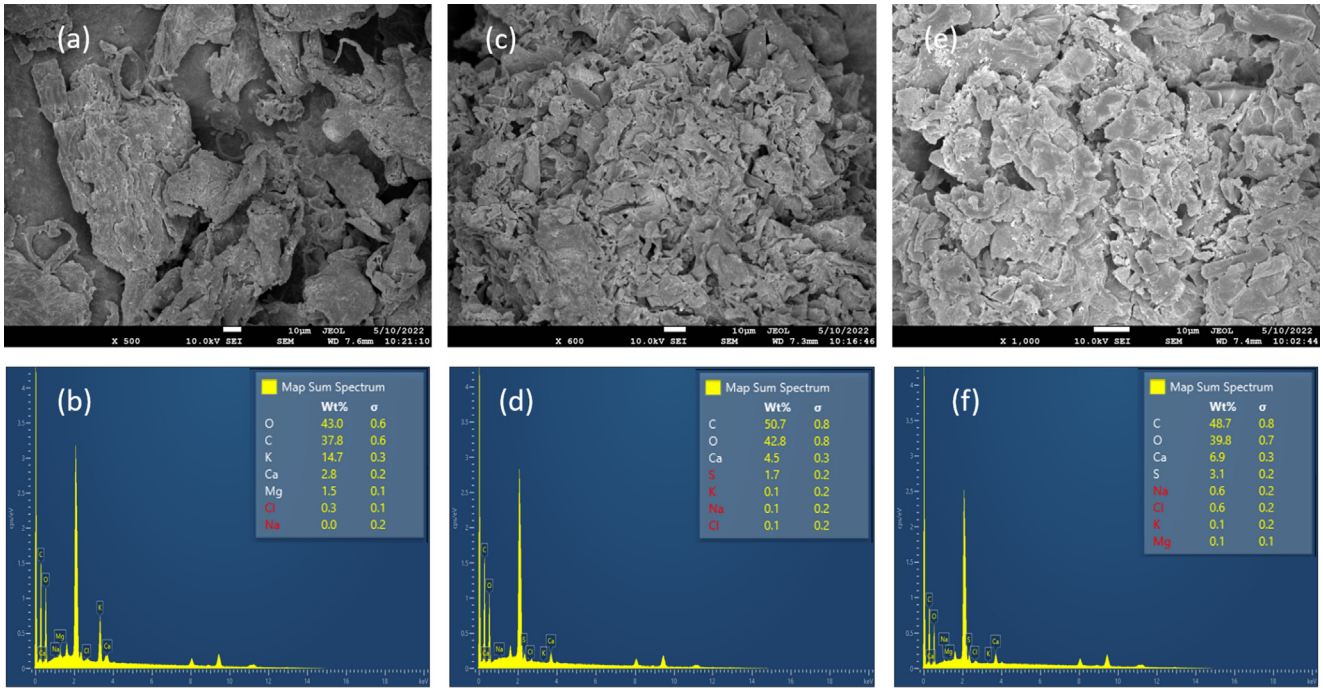

Fig. 4. SEM images of LPP (a), G-LPP (c), and RR 195/G-LPP (e); EDX images of LPP (b), G-LPP (d), and RR 195/G-LPP (f).

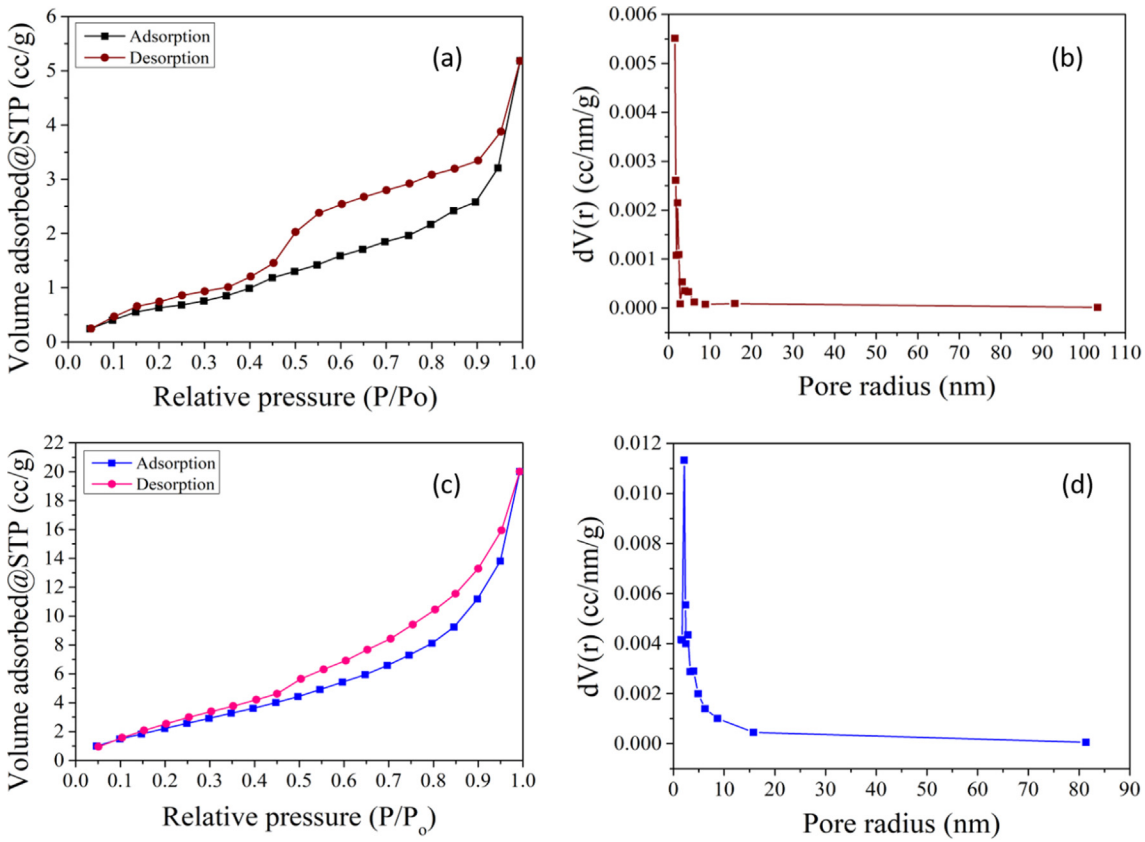

Fig. 5. N_2 adsorption–desorption isotherms of LPP (a), and G-LPP (c); pore size distribution curves of LPP (b), and G-LPP (d).

higher number of $-OH_2^+$ and $-NH_3^+$ ions result in enhanced sorption sites. As a consequence, electrostatic attractions between negatively charged sulfonic ions ($-SO_3^-$) of RR 195 and positively charged protonated hydroxyl and amine increase the adsorption ability at lower pH. On the other hand, when the solution pH rises beyond 4.0, the protonated degree of amine and hydroxyl groups decreases, and electrostatic interactions between RR 195 dye and the surface of G-LPP was weakened, resulting in a decreased removal ability of

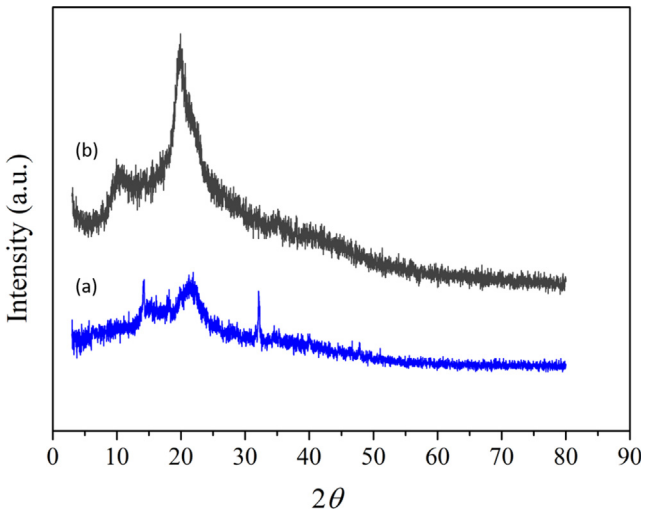

Fig. 6. XRD pattern of the LPP (a) and G-LPP (b).

RR 195. Using a pH_{PZC} (point of zero charge), the adsorption behavior of dye may be readily accessible. pH_{PZC} was an essential parameter that defined the surface's kinetic properties. Generally, pH < pH_{PZC} encourages for sorption of anions, and pH > pH_{PZC} encourages for cations [41]. The pH_{PZC} of the G-LPP was discovered to be 4.5 (Fig. 7b). Below pH_{PZC} the G-LPP surface becomes positively charged because of pronation of functional groups and above pH_{PZC} the surface turned to negatively charged. As a result, the highest RR 95 dye sorption was discovered to occur at pH 4.0 (pH < pH_{PZC}), which was chosen as the best pH for all further experiments.

3.3. Stirring speed

Stirring speed is a vital variable influencing a biosorption process because it affects solute distribution in the bulk solution and the creation of an exterior boundary layer. The impact of stirring on RR 195 sorption onto G-LPP was investigated at various stirring speeds varying from 0 to 400 rpm, as illustrated in Fig. 7c. With increasing shaking speed from 0 to 200 rpm, the quantity of dye absorbed per unit quantity of adsorbent at equilibrium sorption uptake rose from 6 to 29.3 mg/g. It was also discovered that raising the stirring speed from 0 to 200 rpm enhanced the percent removal from 23 to 94.4%. This may be explained by raising the stirring speed, which reduces the film boundary layer around the particles and so upsurges the exterior film transfer coefficient and hence the sorption efficiency. The degree of stirring lowered boundary layer resistance and improved system mobility. However, when the stirring speed was increased (over 200 rpm), the sorption uptake was shown to decrease. The reduction in sorption capacity with increasing stirring speed was primarily due to the fact that at upper stirring speeds, adsorbed dye molecules were subjected to a strong centrifugal force, causing the bound dye molecules to be desorbed from the adsorbent's surface [42]. Thus, 200 rpm was determined to be the optimum speed and was used in further experiments.

3.4. Effect of G-LPP dosage

Optimizing the adsorbent dose is also an essential aspect of the adsorption experiment; the goal is to decrease expenses and maximize the adsorbent used. The impact of adsorbent dosage on percentage removal (%) and adsorption uptake (q_e) of RR 195 is illustrated in Fig. 7d, where other parameters are kept constant. From this figure, by raising the adsorbent dosage from 10 to 50 mg/30 mL, the removal rate of RR 195 continuously grows from 49 to 94.5%, respectively. This increase in the percentage removal of RR 195 was due to the greater contact surface area of the biosorbent and the availability of more sorption sites. Nevertheless, no influence of G-LPP dosage was observed on RR 195 elimination from solution when the mass of adsorbent rose from 50 to 80 mg/30 mL. This means that the adsorption reaches equilibrium

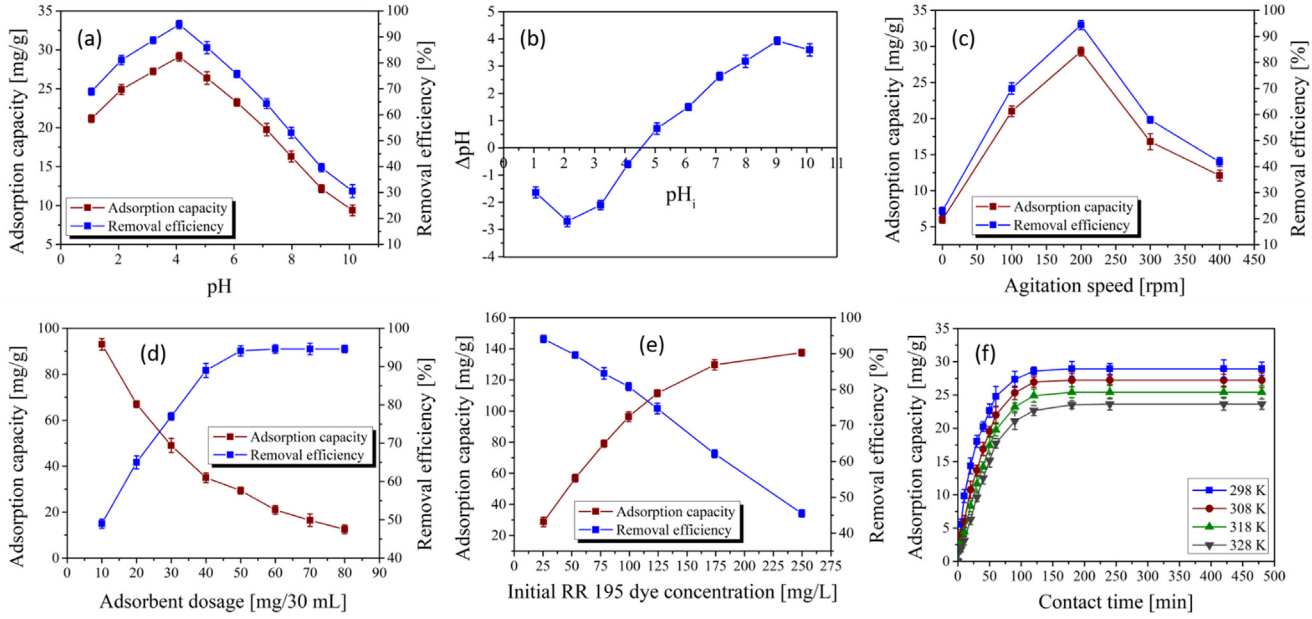

Fig. 7. (a) Effect of pH [pH range: 1.0–10.0, dosage: 50 mg, C_o: 25 mg/L, dye volume: 30 mL, agitation speed: 200 rpm, time: 120 min, temperature: 298 K], (b) Point of zero charge [pH range: 1–10, electrolyte volume: 30 mL, dosage: 50 mg, agitation speed: 120 rpm, time: 24 h, temperature: 298 K] (c) Effect of agitation speed [pH: 4.0, speed range: 0–400 rpm, C_o: 25 mg/L, dosage: 50 mg, dye volume: 30 mL, agitation speed: 200 rpm, temperature: 298 K], (d) Effect of dosage [dosage range: 10–80 mg, pH: 4.0, C_o: 25 mg/L, dye volume: 30 mL, agitation speed: 200 rpm, time: 120 min, temperature: 298 K], (e) Effect of initial dye concentrations [C_o range: 25–250 mg/L, pH: 4.0, dosage: 50 mg, dye volume: 30 mL, agitation speed: 200 rpm, time: 120 min, temperature: 298 K], and (f) Effect of contact time [time: 0–480 min, C_o: 25 mg/L, pH: 4.0, dosage: 50 mg, dye volume: 30 mL, agitation speed: 200 rpm, temperature range: 298–328 K].

between RR 195 molecules on G-LPP and non-adsorbed RR 195 molecules in the solution [43]. On the other hand, the adsorbent uptake remarkably decreased from 93 to 12.5 mg/g while increasing the G-LPP dosage from 10 to 80 mg/30 mL (Fig. 7d). A reduction in adsorption uptake by raising the sorbent mass was due to a larger surface area at the low sorbent mass and resultantly, more collision between particles of sorbent sites and dye molecules. The second one, a rise in sorbent mass at constant dye volume and concentration leads to saturation of active sites, and due to particulate interaction like as aggregates formation at greater sorbent mass could reduce sorption efficiency because aggregation would lead to a reduction in total surface area of the sorbent and reduced diffusion path length [44]. As a result, 50 mg/30 mL of G-LPP adsorbent was selected to adsorb RR 195 in subsequent experiments.

3.5. Impact of initial RR 195 concentration

The impact of the initial RR 195 dye concentration on the biosorption by G-LPP was studied. The adsorption uptake (q_e) and removal efficiency (%) versus different RR 195 dye concentrations are displayed in Fig. 7e. When the initial concentration was raised from 25 to 250 mg/L, the q_e of G-LPP rose from 28.8 to 137.6 mg/g. This might be because the increase in initial dye concentration results in an influential driving force that overcomes the mass transfer barrier between the aqueous and solid phases [44]. However, when RR 195 concentration increased from 25 to 250 mg/L, the % of G-LPP reduced from 94.1 to 45.5%. It may be stated that the existence of adequate active regions on the adsorbent surface is the cause for getting high removal efficiencies at low dye concentrations. The removal efficiency was decreased at higher concentrations because the dye competed for the sorbent's active binding sites and there was inadequate free space to attach the dye molecules to the biosorbent surface [45]. According to obtained results, 25 mg/L was chosen as the optimal initial RR 195 concentration for further studies.

3.6. Influence of contact time

Contact time is a key variable in the adsorption process that estimates the contact time necessary to attain adsorption equilibrium. The effect of RR 195 adsorption contact time on G-LPP was studied at various temperatures (298–328 K) in RR 195 solution with an initial concentration of 25 mg/L. Fig. 7f depicts the variations in adsorption efficiency at various time periods. The adsorption effectiveness of RR 195 improved with increasing contact time, and equilibrium was attained after 120 min. There was no substantial change in adsorption efficiency with time after equilibrium. Because more active sites were originally available on the surface of the G-LPP and the mass transfer impedance of RR 195 dye between aqueous and solid phases was overcome, dye removal progressively increased with contact time. At some point (after 120 min), all of the active sites on the G-LPP surface would be saturated, and no further RR 195 dye removal would occur [38]. The amount of RR 195 dye molecules adsorbed on the surface of G-LPP reduced from 29 to 24 mg/g when the temperature increased from 298 to 328 K. This can have explained by the fact that the adsorbed RR 195 dye molecule moves easily at a lower temperature. Based on these findings, 120 min was selected as the optimal contact time for further tests.

3.7. Adsorption kinetics

Adsorption dynamics define the rate of solute efficiency, and this rate obviously influences the residence time of adsorbate efficiency at the liquid–solid interface. The RR 195 dye adsorption kinetics from the liquid to the solid phase is thought to be a reversible process with an equilibrium state maintained between the two phases. The adsorption mechanism is determined by the adsorbent's physical and chemical characteristics, as well as the mass transfer process. To peruse the governing mechanism of the adsorption, pseudo-first-order (PFO), pseudo-second-order (PSO), and Elovich models were employed using obtained experimental data at several temperatures (298–328 K). The non-linear mathematical models are expressed by the following equations:

$$q_t = q_{e1}(1 - \exp(-k_1 t)) \tag{5}$$

$$q_t = \frac{q_{e2}^2 k_2 t}{1 + q_{e2} k_2 t} \tag{6}$$

$$q_t = \frac{1}{\beta} \ln(1 + \alpha\beta t) \tag{7}$$

Fig. 8 and Table 1 show the non-linear fitting plots and significant constants of the model obtained by applying kinetic data to kinetic model equations. The results showed that the PSO and Elovich models could not provide a non-linear regression and could not explain the experimental data. According to R^2 values of more than 0.9918 for each temperature, the PFO model was highly correlated with experimental results of RR 195 adsorption. Aside from the R^2 values, the closeness of theoretically calculated ($q_{e,\ cal}$) and experimentally acquired ($q_{e,\ \exp}$) maximum adsorption capacity suggests that the PFO model was suitable for defining adsorption kinetic data. The good fitness of the PFO model implied that the adsorption of RR 195 onto G-LPP was controlled by a physisorption process [46].

3.8. Arrhenius activation energy

At various temperatures, the Arrhenius equation is used to associate the rate constant and activation energy of the kinetic model. In linear form, the Arrhenius equation may be represented as follows:

$$\ln k_2 = \ln A_o - \frac{E_a}{RT} \tag{8}$$

The sort of interactions between RR 195 and G-LPP is often described by the chemical or physical adsorption process. The magnitude of E_a indicates whether the adsorption is mostly physical or chemical. Physisorption is a process in which the energy required is such that the E_a is between 5.0 and 40 kJ/mol. As a result of the modest intermolecular interactions involved, the process interaction in such a system is readily reversible, and equilibrium is quickly established. Chemisorption experiences stronger bonding forces, resulting in a high process activation energy range of 40–80 kJ/mol [47]. A linear plot of $1/T$ vs. ln k_2 for the adsorption of RR 195 onto G-LPP (Fig. 9) was built to calculate the activation energy from the slope ($-E_a/R$). The adsorption of RR 195 onto G-LPP yielded a value of 16.3 kJ/mol, showing that the adsorption has a low potential barrier and corresponds to physisorption. This supports the observation that the process followed PFO.

3.9. Adsorption isotherm modelling

Equilibrium adsorption plots depict the relationship between the quantity of adsorbate adsorbed on a given biosorbent surface and the equilibrium concentration of the substrate in isothermal contact with the adsorbent. In the present study, four adsorption isotherms, namely: Temkin, Langmuir, D-R (Dubinin-Radushkevich), and Freundlich models, were employed to understand the sorption mechanism and for the non-linear fit of the batch equilibrium data.

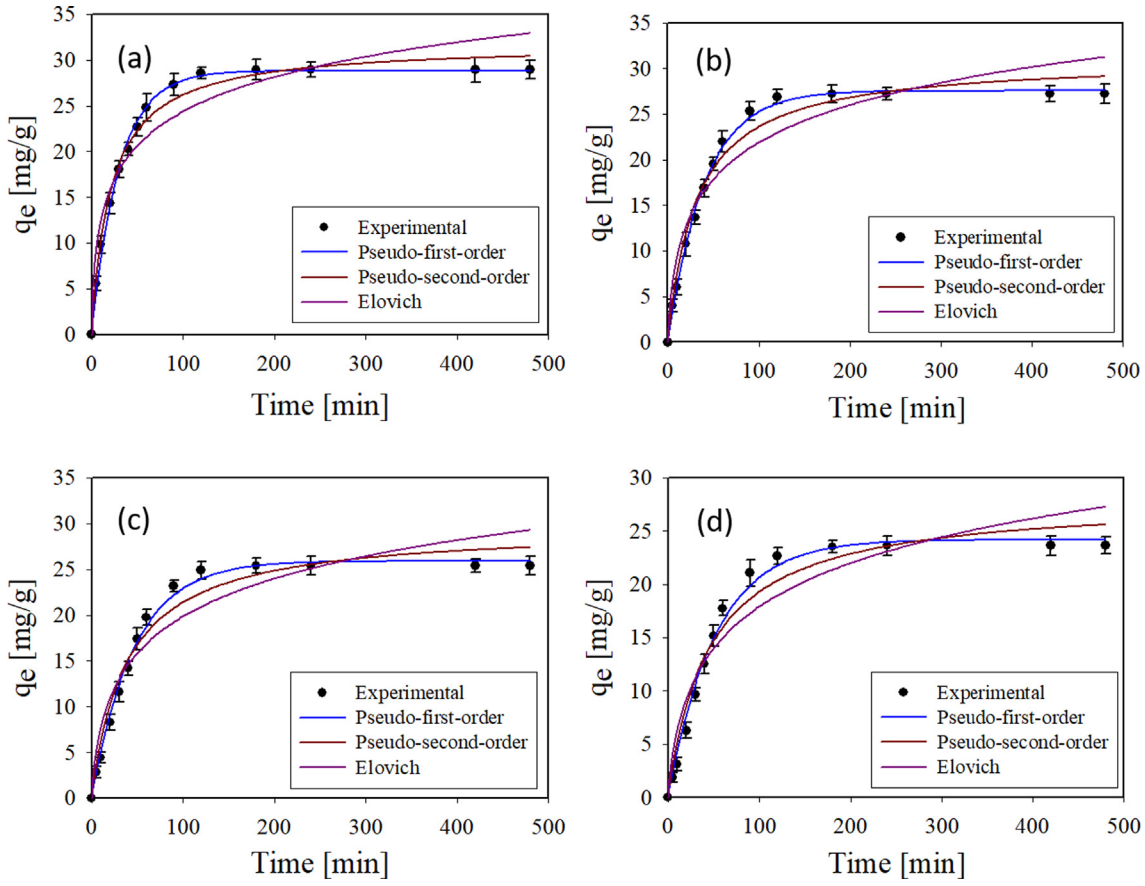

Fig. 8. Non-linear plots of different kinetic models at (a) 298 K; (b) 308 K; (c) 318 K and (d) 328 K for the adsorption of RR 195 onto G-LPP [C_o: 25 mg/L, pH: 4.0, dosage: 50 mg, dye volume: 30 mL, agitation speed: 200 rpm, temperature range: 298–328 K].

Table 1
Kinetic parameters for the adsorption of RR 195 onto G-LPP.

Kinetic Model	Kinetic parameters	Temperature [K]			
		298	308	318	328
Experimental value	$q_{e,\ exp}$ (mg/g)	28.93	27.23	25.42	23.98
Pseudo-first-order	$q_{e1,\ cal}$ (mg/g)	28.83	27.57	25.91	24.18
	k_1 (1/min)	0.0333	0.0249	0.0216	0.0192
	R^2	0.9918	0.9973	0.9959	0.9951
Pseudo-second-order	$q_{e2,\ cal}$ (mg/g)	31.77	31.04	29.58	28.01
	k_2 (g/mg min)	0.0015	0.0012	0.001	0.0008
	R^2	0.9890	0.9779	0.9716	0.9662
Elovich	α (mg/g min)	4.623	2.215	1.507	1.076
	β (g/mg)	0.182	0.166	0.163	0.158
	R^2	0.9290	0.9219	0.9183	0.9153

The Langmuir equation has been frequently used to explain experimental sorption data. It is based on the idea that adsorption occurs on a homogenous surface by monolayer sorption with no contact between biosorbent molecules. The model assumes homogeneous adsorption energies on the surface and no adsorbate transmigration in the plane of the surface. The Langmuir model may be represented in non-linearized form as follows:

$$q_e = \frac{q_{\max} K_L C_e}{1 + K_L C_e} \tag{9}$$

The decrease of q_{max} values from144.9 to 124.2 mg/g with an increment of solution temperature from 298 to 328 K suggested that the biosorption of RR 195 onto G-LPP was exothermic (i.e., the dye-adsorbent interaction was more energetic at low temperature) [48]. The values of the isotherm constant (K_L) of RR 195 dye range from 0 to 1 (Table 2), showing that the adsorption of RR 195 onto G-LPP is advantageous [49].

The basic properties of the Langmuir isotherm factors may be utilized to predict the affinity between the sorbent and sorbate using the dimensionless equilibrium variable or separation factor, R_L, defined as in Eq. (10):

$$R_L = \frac{1}{(1 + K_L C_o)} \tag{10}$$

The R_L values specify the type of the adsorption process to be favourable ($0 < R_L < 1.0$), unfavourable ($R_L > 1.0$), linear ($R_L = 1.0$), and irreversible ($R_L = 0$) [8]. In the present study, as shown in Table 3, R_L values were between $0 < R_L < 1.0$, which confirmed that the sorption of RR 195 onto G-LPP was favorable.

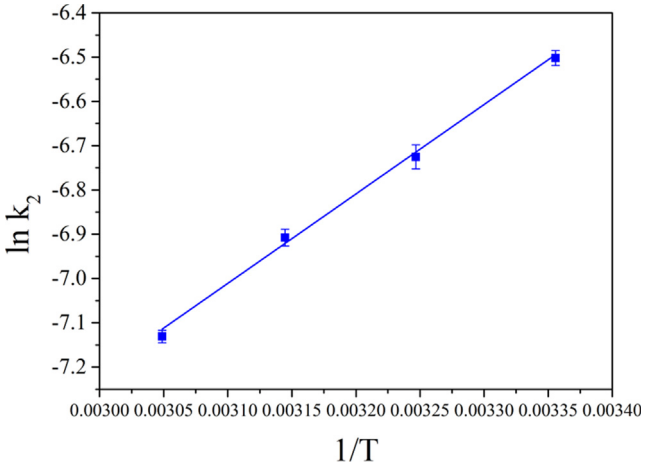

Fig. 9. Arrhenius plot for adsorption of RR 195 onto G-LPP.

The Freundlich model illustrates the link between reversible and non-ideal adsorption and is used to represent adsorption on a heterogeneous surface with interactions between adsorbed molecules. The Freundlich equation also shows that sorption energy falls exponentially when the adsorbent's sorption centers are completed. The non-linear form of this equation is:

$$q_e = K_f C_e^{1/n} \tag{11}$$

The '*n*' value in the Freundlich model reflects the degree of non-linearity between solution concentration and adsorption as follows: if $n > 1.0$, then sorption is physisorption; if $n < 1.0$, then sorption is chemisorption; if $n = 1.0$, then sorption is linear [50]. In this work, the exponent *n* values at all temperatures were>1.0 (Table 2); this indicates the adsorption of RR 195 onto G-LPP is physisorption.

The Temkin model includes a factor that explicitly accounts for the interactions between adsorbate and adsorbent. The heat of sorption of all molecules in the layer is considered to reduce linearly with coverage in this equation because of these interactions, neglecting extremely low and very high concentration values. The Temkin model is expressed in its non-linearized form as follows:

$$q_e = B_T \ln(A_T C_e) \tag{12}$$

$$q_e = B_T \ln(A_T) + B_T \ln(C_e) B_T = \frac{RT}{b_T} \tag{14}$$

The variability in B_T and A_T values with increasing working solution temperature suggests that the energy and binding energy of adsorption for RR 195 sorption are influenced by a change in temperature. According to the Temkin isotherm, the energy of sorption, $A_T < 8.0$ kJ/mol, represents typical physical sorption, while the range $8.0 > A_T < 16.0$ kJ/mol represents an ion-exchange mechanism [51]. The obtained A_T values (1.996–0.522) from the Temkin isotherm model were under < 8.0 kJ/mol (Table 2), indicating the adsorption of RR 195 by G-LLP via physisorption. In the physisorption process, the adsorbate adheres to the biosorbent through weak Van der Walls interactions and thus this process is associated with relatively low adsorption energies [52].

The Dubinin-Radushkevich model does not make any assumptions about a homogeneous surface or a constant sorption potential. It is used to assess the nature of the sorption process as well as the mean energy of sorption. The equation for the D-R model is as follows:

$$q_e = q_s \exp(-K\varepsilon^2)\varepsilon = RT \ln\left(1 + \frac{1}{C_e}\right) \tag{16}$$

The *E*, mean free sorption energy, is calculated from Eq. (17):

$$E = \frac{1}{\sqrt{2K}} \tag{17}$$

The *E* value is used to define the adsorption type: physisorption if the *E* value is $1.0 < E < 8.0$ kJ/mol; ion exchange if the *E* value is between 8.0 and 16.0 kJ/mol; and chemisorption if the *E* value is>16 kJ/mol [53]. In the current work, the calculated *E* values ranged between $1.0 < E < 8.0$ kJ/mol (Table 2), which indicates that the adsorption of RR 195 onto G-LPP occurred through the physisorption.

Fig. 10 displays the fitting curves of isotherms and the obtained variables of the isotherm models are presented in Table 2. The lower χ^2 and higher R^2 values from Table 2 clearly demonstrate that the data could be well fitted by the Langmuir model compared to the other isotherm models. It indicates that a monolayer coverage of RR 195 is adsorbed onto the homogeneous surface of the G-LPP.

3.10. Comparison of the maximum RR 195 adsorption of various sorbents

In order to evaluate the adsorption performance of G-LPP toward RR 195 anionic dye, its maximum adsorption efficiency (q_{max}) was compared with some other reported ones in the litera-

Table 2
Different isotherm parameters for the adsorption of RR 195 onto G-LPP.

Isotherm model	Isotherm parameters	Temperature (K)			
		298	308	318	328
Langmuir	q_m (mg/g)	144.9	137.7	130.1	124.2
	K_L (L/mg)	0.112	0.103	0.073	0.054
	R^2	0.9939	0.9979	0.9918	0.9899
	χ^2	16.8	5.1	16.7	17.5
Freundlich	K_f (mg/g)	39.27	36.8	29.98	23.57
	n	3.67	3.71	3.44	3.13
	R^2	0.9605	0.9336	0.9195	0.9283
	χ^2	108.9	162.7	164.6	124.8
Temkin	B_T (J/mol)	96.5	98.7	100.1	102.8
	A_T (L/mg)	1.996	1.416	0.802	0.522
	R^2	0.9859	0.9619	0.9426	0.9535
	χ^2	25.9	60.7	75.2	51.8
D-R	q_s (mg/g)	120.6	116.1	105.4	97.8
	K (mol^2/J^2)	0.07	0.08	0.09	0.11
	E (kJ/mol)	2.7	2.5	2.4	2.1
	R^2	0.7969	0.8552	0.8093	0.8206
	χ^2	374.8	330.8	218.7	188.4

Table 3
R_L values based on the Langmuir equation.

RR 195 C_o (mg/L)	R_L values at different temperatures (K)			
	298	308	318	328
25	0.263	0.279	0.354	0.426
50	0.152	0.163	0.215	0.270
75	0.106	0.115	0.154	0.198
100	0.082	0.088	0.121	0.156
125	0.067	0.072	0.099	0.129
175	0.049	0.053	0.073	0.096
250	0.037	0.037	0.052	0.069
Average value of R_L	0.108	0.115	0.153	0.192

ture [3,6,54–61], as summarized in Table 4. It can be found that G-LPP acts significantly higher than other reported adsorbents and can be a promising biosorbent for the removal of RR 195 from aquatic environments.

3.11. Effect of temperature

The temperature plays a vital role in determining whether the sorption process is exothermic or endothermic. The impact of temperature on the adsorption of RR 195 by G-LPP was analyzed at different temperatures and the results are displayed in Fig. 11a. It was noticed that the adsorption capacity and removal efficiency was

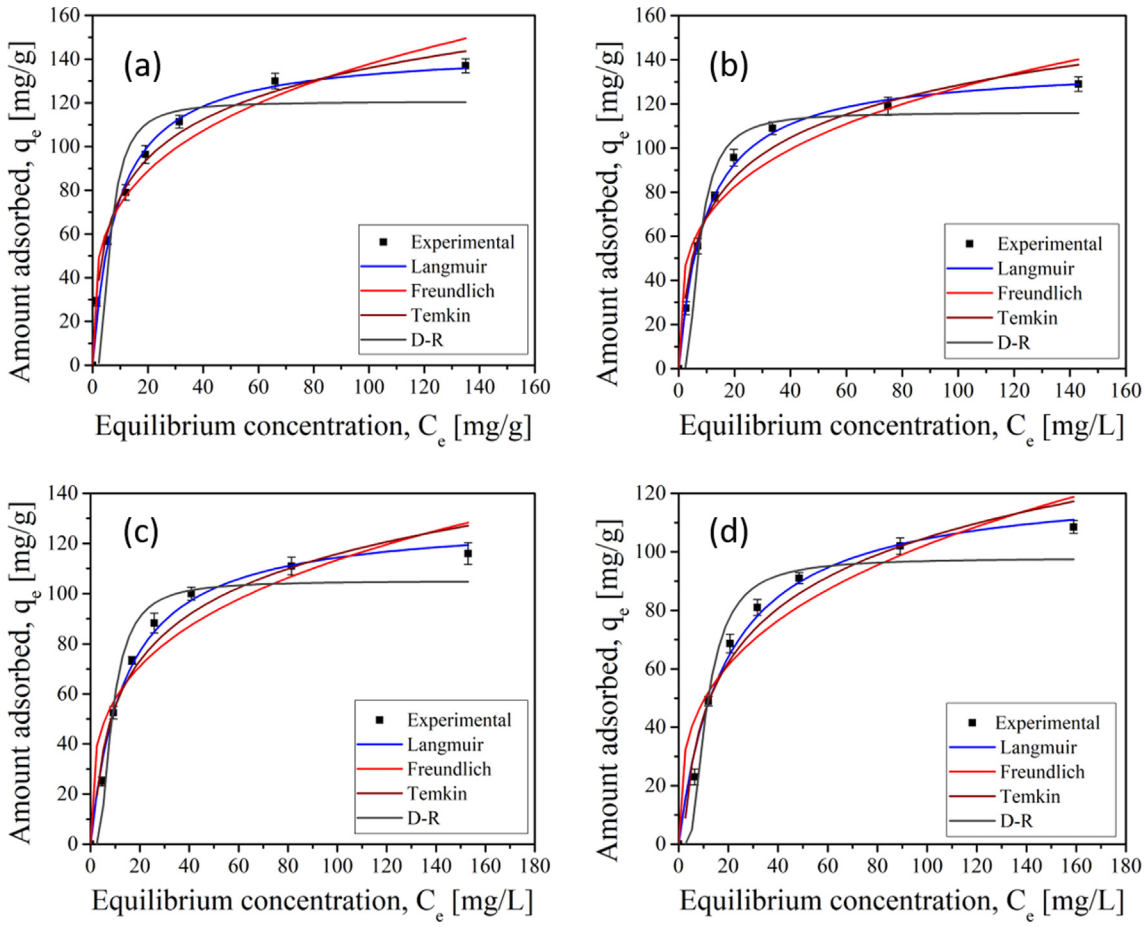

Fig. 10. (a) Effect of temperature [temperature range: 298–328 K, C_o: 25 mg/L, dye volume: 30 mL, dosage: 50 mg, pH: 4.0, agitation speed: 200 rpm, time:120 min] and (b) Van't Hoff plot for the adsorption of RR 195 onto G-LPP [temperature range: 298–328 K, C_o: 25 mg/L, dye volume: 30 mL, pH: 4.0, dosage: 50 mg, agitation speed: 200 rpm, time:120 min].

Table 4
Comparison of the adsorption performance of RR 195 for different types of materials.

Adsorbent	pH	Initial dye concentration (mg/L)	Temperature (K)	Removal (%)	q_{max} (mg/g)	Reference
Chitosan coacervated particles	4.0	40–500	298	85.6	63.2	[3]
NaOH treated jute fibre	7.0	10–120	293	–	28.14	[6]
Dehydrated beet pulp carbon	1.0	20–100	323	94	58	[54]
Biomass of *Pinus sylvestris* Linneo	4.0	50–200	293	98.8	8.425	[55]
Wheat bran	1.5	50–150	293	–	103.3	[56]
Barberry stem (ash)	3.0	10–50	288	–	8.8	[57]
Barberry stem (powder)	3.0	10–50	288	–	27.2	[57]
Dimethylamine modified lotus leaf powder	2.0	100–1000	298	–	131.5	[58]
TiO_2 nanoparticles	3.0	10–75	303	~ 100	~ 87	[59]
α-Fe_2O_3 nanoparticles	2.0	10–50	298	98.77	4.7	[60]
Soybean leaves modified with acetic acid	–	5–40	323	97.8	12	[61]
Glycidyltrimethylammonium chloride modified-Lychee peel powder (G-LPP)	4.0	25–250	298	94.5	144.9	Present study

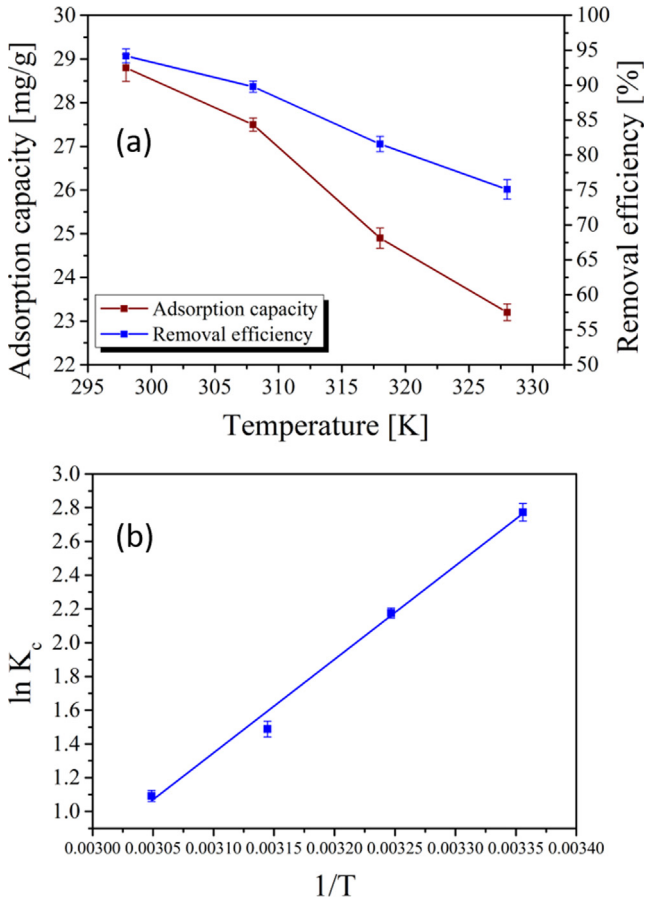

Fig. 11. Non-linear plots of different isotherm models at (a) 298 K; (b) 308 K; (c) 318 K and (d) 328 K for the adsorption of RR 195 onto G-LPP [C_o: 25–250 mg/L, pH: 4.0, dosage: 50 mg, dye volume: 30 mL, agitation speed: 200 rpm, temperature range: 298–328 K].

decreased with an increase in the solution temperature from 298 to 328 K, indicating clearly that RR 195 is adsorbed exothermically onto G-LPP. This might be attributed to the weakening of binding interactions which aids in the detachment of dye molecules from the surface of the sorbent causing reduced dye adsorption at elevated temperatures [62]. These findings suggested that the sorption process is more feasible and favorable at room temperature (298 K) than at higher temperatures (308, 318, and 328 K).

3.12. Thermodynamic analysis

Thermodynamics is a commonly used method in the study of adsorption behavior, with the goal of better understanding the impacts of temperature on sorption processes and their nature. The thermodynamic factors such as a change in entropy (ΔS^o), enthalpy (ΔH^o), and Gibbs free energy (ΔG^o) can be evaluated from the following Van't Hoff equations:

$$\Delta G^o = \Delta H^o - T\Delta S^o \tag{18}$$

$$\Delta G^o = -RT \ln K_c \tag{19}$$

$$K_c = \frac{C_{Ae}}{C_e} \ln K_c = -\frac{\Delta G^o}{RT} = -\frac{\Delta H^o}{RT} + \frac{\Delta S^o}{R} \tag{21}$$

The thermodynamic factors for the adsorption of RR 195 onto G-LPP are summarized in Table 5. The slope ($-\Delta H^o/R$) and intercept ($\Delta S^o/R$) of the linear plot of $1/T$ vs. ln K_C displayed in Fig. 11b were

Table 5
Thermodynamic parameter for the adsorption of RR 195 onto G-LPP.

Temperature [K]	Thermodynamic parameters		
	ΔG^o (kJ/mol)	ΔS^o (J/mol K)	ΔH^o (kJ/mol)
298	−6.8693		
308	−5.5718	−133	−46.6
318	−3.9351		
328	−2.9777		

used to calculate the values of ΔS^o and ΔH^o. At all temperatures, the negative value of ΔG^o shows that the sorption process of RR 195 onto G-LPP is spontaneous. The ΔG^o value rose as the temperature was raised from 298 to 328 K (Table 5). This means that the spontaneity of the adsorption process will decrease as the temperature increases [63]. Generally, ΔG^o values range from −80.0 to −400.0 kJ/mol for chemisorption and 0 to −20.0 kJ/mol for physisorption. Therefore, based on the ΔG^o values, the adsorption of RR 195 onto the G-LPP surface refers to physisorption. The negative value of ΔH^o indicates that the adsorption is exothermic, explaining the adsorption is unfavorable with the increase in temperature [64]. On the other hand, the negative value of ΔS^o reflects a reduction in the degree of freedom of absorbed species at the liquid–solid interface [65]. In a word, the ΔG^o, ΔH^o, and ΔS^o all are negative, which indicates that the adsorption occurs spontaneously at low temperatures.

3.13. Regeneration and reusability of the G-LPP

Adsorbent reusability is an important consideration in determining economic viability. To do this, the adsorbent was first regenerated with different solvents and then re-used over numerous cycles to check whether there was any performance degradation. For regeneration (Fig. 12a), eight distinct solvents were used: 0.1 M H_2SO_4, 0.1 M NaCl, 0.1 M HCl, 0.1 M HNO_3, 0.1 M NaOH, methanol, ethanol, and acetone. The eluents employed in regeneration have the following possibilities: NaOH (91.2%) > NaCl (69.6%) > HCl (65.2%) > methanol (58.4%) > H_2SO_4 (48.1%) > acetone (45.5%) > ethanol (39.2%) > HNO_3 (31.6%). NaOH was used to desorb RR 195 dye molecules from G-LPP across numerous cycles since it caused improved desorption. The results of five sequential adsorption/desorption cycles used to determine reusability are shown in Fig. 12b. Between the 1st and 2nd cycles, the RR 195 adsorption efficiency declined from 94.5 to 91.2 %. In the 5th cycle, the RR 195 adsorption efficiency declined to 77.3%. This might be owing to the reduced RR 195 uptake by the G-LPP, which indicated a loss in regeneration efficiency for continuous regeneration cycles. The reduction might also be attributed to a reduction in the number of binding sites on the G-LPP surface [66]. Furthermore, RR 195 dye molecules might have saturated the available binding sites on the biosorbent. Desorption efficiency for RR 195 has similarly declined from 91.2% in the 1st cycle to 74.7% in the 5th cycle. Desorption efficiency was lower than adsorption efficiency for all cycles due to the repeated cycle of adsorption (or) desorption. This mechanism might have led to heterogeneity on the surface of the G-LPP. Meanwhile, a sturdy interaction is achievable between RR 195 dye molecules and binding sites with higher energy. These findings demonstrated that G-LPP has a strong regeneration ability and may be utilized for the RR 195 adsorption/desorption process indefinitely.

3.14. Adsorption mechanism

Adsorption of dye molecules on the biosorbent surface can be ion exchange, chemical, or physical. The kinetics (PFO), activation

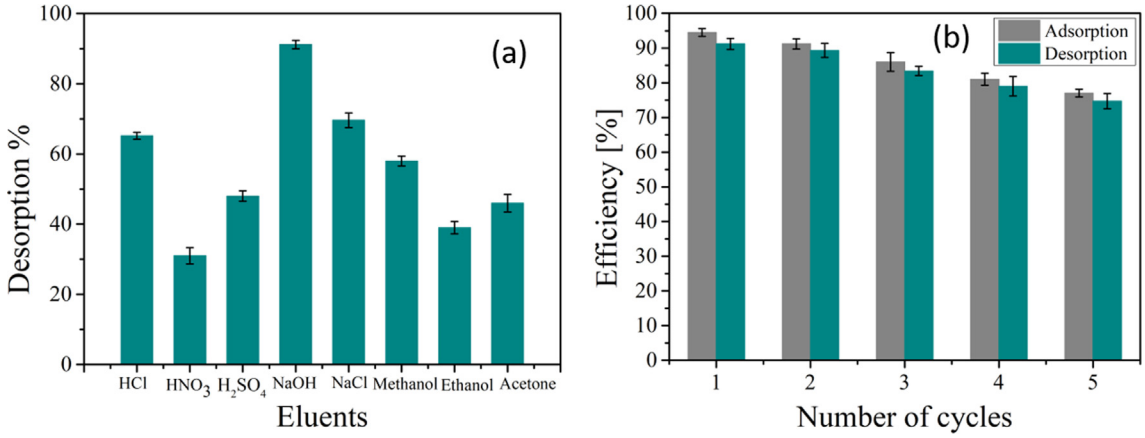

Fig. 12. (a) Desorption and (b) Reusability studies for G-LPP by RR 195 dye.

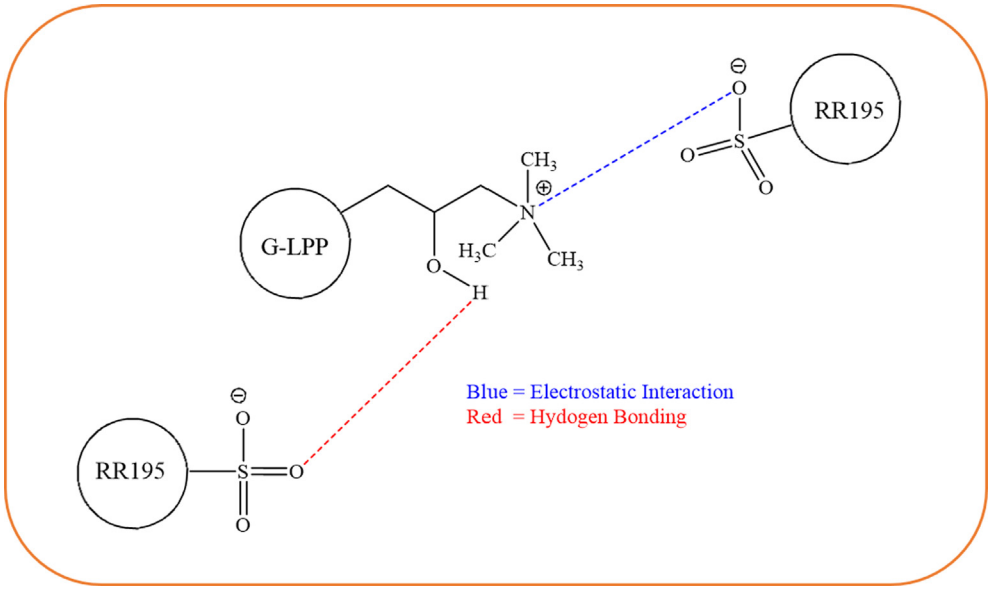

Fig. 13. The possible interaction mechanism between the RR 195 and G-LPP.

energy, isotherms (D-R, Temkin, and Freundlich), and thermodynamic (Gibbs free energy) parameters, indicate that the G-LPP adsorbed RR 195 dye molecule through the physisorption. The proposed adsorption mechanism for the adsorption of RR 195 onto G-LPP is illustrated in Fig. 13. The main functional groups involved in the adsorption mechanisms are –OH and $–NH_2$. Since the optimal removal of RR 195 by G-LPP occurs in solution at pH 4.0, the positively charged groups of G-LPP can promote the electrostatic attraction with the negatively charged ($-SO_3^-$) groups of RR 195. Moreover, hydrogen bonding interaction was also involved in the adsorption mechanism. The hydrogen bonding between the –OH group of G-LPP and the O atom of the RR 195 dye molecule could be attributed to the adsorption of the RR 195 dye molecule. As a result, the adsorption mechanism of G-LPP for RR 195 was the main physisorption, while electrostatic interaction and hydrogen bonding also played significant roles.

4. Conclusions

Quaternary ammonium-modified lychee peel powder was successfully prepared and employed for the elimination of RR 195 from the waste effluents. The RR 195 adsorption process was found to be influenced by solution pH, G-LPP mass, temperature, contact time, stirring speed, and initial dye concentration. The prepared adsorbents (LLP, G-LPP, and RR 195/G-LPP) were characterized by BET/BJH, FE-SEM/EDX, XRD, pH_{PZC}, and FTIR analyses. The FT-IR analyses revealed the presence of a quaternary ammonium group, indicating the successful modification of GTMAC onto the LPP surface. The XRD results show that the prepared G-LPP has an amorphous structure. The FE-SEM morphology shows the rough and porous structure on the surface of the G-LPP, which can provide enhanced accessibility for RR 195 dye molecules. The results from the BET surface area showed that the modification of LPP by GTMAC increased the surface area from 2.813 to 17.48 m^2/g (6.2 times). The adsorption process of RR 195 onto G-LPP followed the Langmuir isotherm model and the PFO kinetics, indicating that it was monolayer adsorption and mainly controlled by physical action. The high percentage removal of RR 195 was observed in an acidic medium, and the highest removal was recorded at pH 4.0. The maximum adsorption capacities of 144.9, 137.7, 130.1, and 124.2 mg/g were obtained at temperatures 298, 308, 318, and 328 K respectively, which indicated that RR 195 adsorption onto G-LPP is exothermic. The value of E_a for the adsorption of RR 195 onto G-LPP was found to be 16.3 kJ/mol, suggesting that

physisorption was the predominant mechanism involved. The thermodynamic factors showed a favorable, spontaneous, and exothermic adsorption system. Besides, the adsorption–desorption system displayed more stability than the G-LPP structure and can be recycled for up to five cycles. The hydrogen bonding and electrostatic interactions may significantly dominate RR 195 dye removal. It may be concluded from the reported observations that G-LPP has the potential to be used as an efficient, economically feasible, and low-cost sorbent for the elimination of RR 195 dye from an aqueous solution and real colored wastewater.

CRediT authorship contribution statement

Venkata Subbaiah Munagapati: Writing – original draft, Data curation, Methodology, Conceptualization, Visualization, Formal analysis. **Hsin-Yu Wen:** Conceptualization, Validation, Visualization. **Anjani R.K. Gollakota:** Data curation, Formal analysis, Conceptualization. **Jet-Chau Wen:** Conceptualization, Supervision, Resources, Funding acquisition, Data curation, Writing – review & editing. **Kun-Yi Andrew Lin:** Data curation, Visualization, Writing – review & editing. **Chi-Min Shu:** Conceptualization, Writing – review & editing. **Guda Mallikarjuna Reddy:** Conceptualization. **Grigory V. Zyryanov:** Conceptualization. **Jhy-Horng Wen:** Conceptualization. **Zhong Tian:** Conceptualization.

Data availability

Data will be made available on request.

Declaration of Competing Interest

The authors declare that they have no known competing financial interests or personal relationships that could have appeared to influence the work reported in this paper.

Acknowledgement

The authors would like to acknowledge the research support from, MOST 107-2625-M-224-002, MOST 108-2625-M-224-005, and MOST 110-2625-M-224-001, by the Ministry of Science and Technology (MOST), Taiwan.

References

[1] P. Ashokan, M. Asaithambi, V. Sivakumar, P. Sivakumar, Batch and column mode adsorption studies of reactive red 195 dye using Adenanthera paronina L seed activated carbon, Groundw. Sustain. Dev. 15 (2021), https://doi.org/10.1016/j.gsd.2021.100671.
[2] U. Tyagi, Adsorption of dyes using activated carbon derived from pyrolysis of vetiveria zizanioides in a fixed bed reactor, Groundw. Sustain. Dev. 10 (2020), https://doi.org/10.1016/j.gsd.2019.100303.
[3] J. Pérez-Calderón, M.V. Santos, N. Zaritzky, Reactive RED 195 dye removal using chitosan coacervated particles as bio-sorbent: Analysis of kinetics, equilibrium and adsorption mechanisms, J. Environ. Chem. Eng. 6 (2018) 6749–6760, https://doi.org/10.1016/j.jece.2018.10.039.
[4] M. Iqbal, Vicia faba bioassay for environmental toxicity monitoring: A review, Chemosphere 144 (2016) 785–802, https://doi.org/10.1016/j.chemosphere.2015.09.048.
[5] J. Pérez-Calderón, M.V. Santos, N. Zaritzky, Synthesis, characterization and application of cross-linked chitosan/oxalic acid hydrogels to improve azo dye (Reactive Red 195) adsorption, React. Funct. Polym. 155 (2020), https://doi.org/10.1016/j.reactfunctpolym.2020.104699.
[6] A.K. Dey, A. Dey, Selection of optimal processing condition during removal of Reactive Red 195 by NaOH treated jute fibre using adsorption, Groundw. Sustain. Dev. 12 (2021), https://doi.org/10.1016/j.gsd.2020.100522.
[7] M.E. Mahmoud, G.M. Nabil, N.M. El-Mallah, H.I. Bassiouny, S. Kumar, T.M. Abdel-Fattah, Kinetics, isotherm, and thermodynamic studies of the adsorption of reactive red 195 A dye from water by modified Switchgrass Biochar adsorbent, J. Ind. Eng. Chem. 37 (2016) 156–167, https://doi.org/10.1016/j.jiec.2016.03.020.
[8] V. Subbaiah Munagapati, H.Y. Wen, J.C. Wen, A.R.K. Gollakota, C.M. Shu, G. Mallikarjuna Reddy, Characterization of protonated amine modified lotus (Nelumbo nucifera) stem powder and its application in the removal of textile (Reactive Red 120) dye from liquid phase, J. Mol. Liq. 338 (2021), https://doi.org/10.1016/j.molliq.2021.116486.
[9] V. Subbaiah Munagapati, H.Y. Wen, A.R.K. Gollakota, J.C. Wen, C.M. Shu, K.Y. Andrew Lin, Z. Tian, J.H. Wen, G. Mallikarjuna Reddy, G.V. Zyryanov, Magnetic Fe_3O_4 nanoparticles loaded papaya (Carica papaya L.) seed powder as an effective and recyclable adsorbent material for the separation of anionic azo dye (Congo Red) from liquid phase: Evaluation of adsorption properties, J. Mol. Liq. 345 (2022), https://doi.org/10.1016/j.molliq.2021.118255.
[10] M.T. Yagub, T.K. Sen, H.M. Ang, Equilibrium, kinetics, and thermodynamics of methylene blue adsorption by pine tree leaves, Water. Air. Soil Pollut. 223 (2012) 5267–5282, https://doi.org/10.1007/s11270-012-1277-3.
[11] V.K. Gupta, Suhas, Suhas, Application of low-cost adsorbents for dye removal - A review, J. Environ. Manage. 90 (8) (2009) 2313–2342.
[12] I. Hachoumi, E. Tatár, V.G. Mihucz, G. Orgován, G. Záray, S. El Antri, S. Lazar, Pod razor (Ensis siliqua) shell powder as cost-effective biomineral for removal of nickel(II), copper(II) and zinc(II) from artificially contaminated industrial wastewater, Sustain. Chem. Pharm. 12 (2019), https://doi.org/10.1016/j.scp.2019.100137.
[13] L. Wang, Y. Wang, F. Ma, V. Tankpa, S. Bai, X. Guo, X. Wang, Mechanisms and reutilization of modified biochar used for removal of heavy metals from wastewater: A review, Sci. Total Environ. 668 (2019) 1298–1309, https://doi.org/10.1016/j.scitotenv.2019.03.011.
[14] J.G. Flores-Garnica, L. Morales-Barrera, G. Pineda-Camacho, E. Cristiani-Urbina, Biosorption of Ni(II) from aqueous solutions by Litchi chinensis seeds, Bioresour. Technol. 136 (2013) 635–643, https://doi.org/10.1016/j.biortech.2013.02.059.
[15] J. Wu, J. Yang, P. Feng, G. Huang, C. Xu, B. Lin, High-efficiency removal of dyes from wastewater by fully recycling litchi peel biochar, Chemosphere 246 (2020), https://doi.org/10.1016/j.chemosphere.2019.125734.
[16] S.N. Jain, P.R. Gogate, Efficient removal of Acid Green 25 dye from wastewater using activated Prunus Dulcis as biosorbent: Batch and column studies, J. Environ. Manage. 210 (2018) 226–238, https://doi.org/10.1016/j.jenvman.2018.01.008.
[17] S.N. Jain, P.R. Gogate, Adsorptive removal of acid violet 17 dye from wastewater using biosorbent obtained from NaOH and H_2SO_4 activation of fallen leaves of Ficus racemosa, J. Mol. Liq. 243 (2017) 132–143, https://doi.org/10.1016/j.molliq.2017.08.009.
[18] R. Lafi, A. Hafiane, Removal of methyl orange (MO) from aqueous solution using cationic surfactants modified coffee waste (MCWs), J. Taiwan Inst. Chem. Eng. 58 (2016) 424–433, https://doi.org/10.1016/j.jtice.2015.06.035.
[19] S.N. Jain, P.R. Gogate, Acid Blue 113 removal from aqueous solution using novel biosorbent based on NaOH treated and surfactant modified fallen leaves of Prunus Dulcis, J. Environ. Chem. Eng. 5 (2017) 3384–3394, https://doi.org/10.1016/j.jece.2017.06.047.
[20] J.S. Cao, J.X. Lin, F. Fang, M.T. Zhang, Z.R. Hu, A new absorbent by modifying walnut shell for the removal of anionic dye: Kinetic and thermodynamic studies, Bioresour. Technol. 163 (2014) 199–205, https://doi.org/10.1016/j.biortech.2014.04.046.
[21] W. Zhang, H. Li, X. Kan, L. Dong, H. Yan, Z. Jiang, H. Yang, A. Li, R. Cheng, Adsorption of anionic dyes from aqueous solutions using chemically modified straw, Bioresour. Technol. 117 (2012) 40–47, https://doi.org/10.1016/j.biortech.2012.04.064.
[22] S. Hokkanen, A. Bhatnagar, M. Sillanpää, A review on modification methods to cellulose-based adsorbents to improve adsorption capacity, Water Res. 91 (2016) 156–173, https://doi.org/10.1016/j.watres.2016.01.008.
[23] K.G. Akpomie, J. Conradie, Efficient synthesis of magnetic nanoparticle-Musa acuminata peel composite for the adsorption of anionic dye, Arab. J. Chem. 13 (2020) 7115–7131, https://doi.org/10.1016/j.arabjc.2020.07.017.
[24] V.S. Munagapati, D.S. Kim, Adsorption of anionic azo dye Congo Red from aqueous solution by Cationic Modified Orange Peel Powder, J. Mol. Liq. 220 (2016) 540–548, https://doi.org/10.1016/j.molliq.2016.04.119.
[25] F. Kong, K. Parhiala, S. Wang, P. Fatehi, Preparation of cationic softwood kraft lignin and its application in dye removal, Eur. Polym. J. 67 (2015) 335–345, https://doi.org/10.1016/j.eurpolymj.2015.04.004.
[26] X. Xu, B. Gao, B. Jin, Q. Yue, Removal of anionic pollutants from liquids by biomass materials: A review, J. Mol. Liq. 215 (2016) 565–595, https://doi.org/10.1016/j.molliq.2015.12.101.
[27] S. Noreen, U. Khalid, S.M. Ibrahim, T. Javed, A. Ghani, S. Naz, M. Iqbal, ZnO, MgO and FeO adsorption efficiencies for direct sky Blue dye: Equilibrium, kinetics and thermodynamics studies, J. Mater. Res. Technol. 9 (2020) 5881–5893, https://doi.org/10.1016/j.jmrt.2020.03.115.
[28] Y. Miyah, M. Benjelloun, A. Lahrichi, F. Mejbar, S. Iaich, G. El Mouhri, R. Kachkoul, F. Zerrouq, Highly-efficient treated oil shale ash adsorbent for toxic dyes removal: Kinetics, isotherms, regeneration, cost analysis and optimization by experimental design, J. Environ. Chem. Eng. 9 (6) (2021) 106694.
[29] A. Stavrinou, C.A. Aggelopoulos, C.D. Tsakiroglou, Exploring the adsorption mechanisms of cationic and anionic dyes onto agricultural waste peels of banana, cucumber and potato: Adsorption kinetics and equilibrium isotherms as a tool, J. Environ. Chem. Eng. 6 (2018) 6958–6970, https://doi.org/10.1016/j.jece.2018.10.063.
[30] S. Rangabhashiyam, S. Lata, P. Balasubramanian, Biosorption characteristics of methylene blue and malachite green from simulated wastewater onto Carica papaya wood biosorbent, Surf. Interfaces 10 (2018) 197–215, https://doi.org/10.1016/j.surfin.2017.09.011.

[31] E.A. Khan, Shahjahan, T.A. Khan, Khan, Adsorption of methyl red on activated carbon derived from custard apple (Annona squamosa) fruit shell: Equilibrium isotherm and kinetic studies, J. Mol. Liq. 249 (2018) 1195–1211.
[32] M. Naushad, A.A. Alqadami, Z.A. AlOthman, I.H. Alsohaimi, M.S. Algamdi, A.M. Aldawsari, Adsorption kinetics, isotherm and reusability studies for the removal of cationic dye from aqueous medium using arginine modified activated carbon, J. Mol. Liq. 293 (2019), https://doi.org/10.1016/j.molliq.2019.111442.
[33] M. Caldera-Villalobos, A.M. Herrera-González, M. del P. Carreón-Castro, Improving the adsorption capacity of Opuntia ficus-indica fruit peels by graft-copolymerization using gamma radiation, Radiat. Phys. Chem. 189 (2021) 109653. doi: https://doi.org/10.1016/j.radphyschem.2021.109653.
[34] M. Forghani, A. Azizi, M.J. Livani, L.A. Kafshgari, Adsorption of lead(II) and chromium(VI) from aqueous environment onto metal-organic framework MIL-100(Fe): Synthesis, kinetics, equilibrium and thermodynamics, J. Solid State Chem. 291 (2020), https://doi.org/10.1016/j.jssc.2020.121636.
[35] A. Aichour, H. Zaghouane-Boudiaf, Single and competitive adsorption studies of two cationic dyes from aqueous mediums onto cellulose-based modified citrus peels/calcium alginate composite, Int. J. Biol. Macromol. 154 (2020) 1227–1236, https://doi.org/10.1016/j.ijbiomac.2019.10.277.
[36] J.X. Yang, G.B. Hong, Adsorption behavior of modified Glossogyne tenuifolia leaves as a potential biosorbent for the removal of dyes, J. Mol. Liq. 252 (2018) 289–295, https://doi.org/10.1016/j.molliq.2017.12.142.
[37] H. Gogoi, T. Leiviskä, J. Rämö, J. Tanskanen, Production of aminated peat from branched polyethylenimine and glycidyltrimethylammonium chloride for sulphate removal from mining water, Environ. Res. 175 (2019) 323–334, https://doi.org/10.1016/j.envres.2019.05.022.
[38] A. Saravanan, S. Karishma, S. Jeevanantham, S. Jeyasri, A.R. Kiruthika, P.S. Kumar, P.R. Yaashikaa, Optimization and modeling of reactive yellow adsorption by surface modified Delonix regia seed: Study of nonlinear isotherm and kinetic parameters, Surf. Interfaces 20 (2020), https://doi.org/10.1016/j.surfin.2020.100520.
[39] S. Vigneshwaran, P. Sirajudheen, M. Nikitha, K. Ramkumar, S. Meenakshi, Facile synthesis of sulfur-doped chitosan/biochar derived from tapioca peel for the removal of organic dyes: Isotherm, kinetics and mechanisms, J. Mol. Liq. 326 (2021), https://doi.org/10.1016/j.molliq.2021.115303.
[40] Z. Chaouki, M. Hadri, M. Nawdali, M. Benzina, H. Zaitan, Treatment of a landfill leachate from Casablanca city by a coagulation-flocculation and adsorption process using a palm bark powder (PBP), Sci. African 12 (2021) e00721.
[41] G. Sarojini, S.V. Babu, M. Rajasimman, Adsorptive potential of iron oxide based nanocomposite for the sequestration of Congo red from aqueous solution, Chemosphere 287 (2022), https://doi.org/10.1016/j.chemosphere.2021.132371.
[42] S. Chowdhury, P. Saha, Adsorption Thermodynamics and Kinetics of Malachite Green onto $Ca(OH)_2$-Treated Fly Ash, J. Environ. Eng. 137 (2011) 388–397, https://doi.org/10.1061/(asce)ee.1943-7870.0000334.
[43] T.A. Saleh, A.M. Elsharif, O.A. Bin-Dahman, Synthesis of amine functionalization carbon nanotube-low symmetry porphyrin derivatives conjugates toward dye and metal ions removal, J. Mol. Liq. 340 (2021), https://doi.org/10.1016/j.molliq.2021.117024.
[44] M. Asif Tahir, H.N. Bhatti, M. Iqbal, Solar Red and Brittle Blue direct dyes adsorption onto Eucalyptus angophoroides bark: Equilibrium, kinetics and thermodynamic studies, J. Environ Chem. Eng. 4 (2016) 2431–2439, https://doi.org/10.1016/j.jece.2016.04.020.
[45] B.T. Gemici, H.U. Ozel, H.B. Ozel, Removal of methylene blue onto forest wastes: Adsorption isotherms, kinetics and thermodynamic analysis, Environ. Technol. Innov. 22 (2021), https://doi.org/10.1016/j.eti.2021.101501.
[46] H. Li, F. Wang, J. Li, S. Deng, S. Zhang, Adsorption of three pesticides on polyethylene microplastics in aqueous solutions: Kinetics, isotherms, thermodynamics, and molecular dynamics simulation, Chemosphere 264 (2021), https://doi.org/10.1016/j.chemosphere.2020.128556.
[47] M.I. Ejimofor, I.G. Ezemagu, V.I. Ugonabo, P.C. Nnaji, V.C. Anadebe, C. Diyoke, M.C. Menkiti, Adsorption kinetics, mechanistic, isotherm and thermodynamics study of petroleum produced water coagulation using novel Egeria radiate shell extract (ERSE), J. Indian Chem. Soc. 99 (3) (2022) 100357.
[48] M. Shakly, L. Saad, M.K. Seliem, A. Bonilla-Petriciolet, N. Shehata, New insights into the selective adsorption mechanism of cationic and anionic dyes using MIL-101(Fe) metal-organic framework: Modeling and interpretation of physicochemical parameters, J. Contam. Hydrol. 247 (2022) 103977.
[49] E.N. Heybet, V. Ugraskan, B. Isik, O. Yazici, Adsorption of methylene blue dye on sodium alginate/polypyrrole nanotube composites, Int. J. Biol. Macromol. 193 (2021) 88–99, https://doi.org/10.1016/j.ijbiomac.2021.10.084.
[50] Q.-u.-A. Khalid, A. Khan, H.N. Bhatti, S. Sadaf, A. Kausar, S.A. Alissa, M.K. Alghaith, M. Iqbal, Cellulosic biomass biocomposites with polyaniline, polypyrrole and sodium alginate: Insecticide adsorption-desorption, equilibrium and kinetics studies, Arab. J. Chem. 14 (7) (2021) 103227.
[51] T.A. Khan, M.d. Nouman, D. Dua, S.A. Khan, S.S. Alharthi, Adsorptive scavenging of cationic dyes from aquatic phase by H_3PO_4 activated Indian jujube (Ziziphus mauritiana) seeds based activated carbon: Isotherm, kinetics, and thermodynamic study, J. Saudi Chem. Soc. 26 (2) (2022) 101417.
[52] C.S.T. Araújo, I.L.S. Almeida, H.C. Rezende, S.M.L.O. Marcionilio, J.J.L. Léon, T.N. de Matos, Elucidation of mechanism involved in adsorption of Pb(II) onto lobeira fruit (Solanum lycocarpum) using Langmuir, Freundlich and Temkin isotherms, Microchem. J. 137 (2018) 348–354, https://doi.org/10.1016/j.microc.2017.11.009.
[53] S. Archana, B.K. Jayanna, A. Ananda, M.S. Ananth, A. Mossad Ali, H.B. Muralidhara, K.Y. Kumar, Numerical investigations of response surface methodology for organic dye adsorption onto Mg-Al LDH -GO Nano Hybrid: An optimization, kinetics and isothermal studies, J. Indian Chem. Soc. 99 (1) (2022) 100249.
[54] A.Y. Dursun, O. Tepe, Removal of Chemazol Reactive Red 195 from aqueous solution by dehydrated beet pulp carbon, J. Hazard. Mater. 194 (2011) 303–311, https://doi.org/10.1016/j.jhazmat.2011.07.105.
[55] O. Aksakal, H. Ucun, Equilibrium, kinetic and thermodynamic studies of the biosorption of textile dye (Reactive Red 195) onto Pinus sylvestris L, J. Hazard. Mater. 181 (2010) 666–672, https://doi.org/10.1016/j.jhazmat.2010.05.064.
[56] F. Çiçek, D. Özer, A. Özer, A. Özer, Low cost removal of reactive dyes using wheat bran, J. Hazard. Mater. 146 (2007) 408–416, https://doi.org/10.1016/j.jhazmat.2006.12.037.
[57] M. Kamranifar, M. Khodadadi, V. Samiei, B. Dehdashti, M. Noori Sepehr, L. Rafati, N. Nasseh, Comparison the removal of reactive red 195 dye using powder and ash of barberry stem as a low cost adsorbent from aqueous solutions: Isotherm and kinetic study, J. Mol. Liq. 255 (2018) 572–577, https://doi.org/10.1016/j.molliq.2018.01.188.
[58] V.S. Munagapati, H.Y. Wen, J.C. Wen, A.R.K. Gollakota, C.M. Shu, K.Y.A. Lin, J.H. Wen, Adsorption of Reactive Red 195 from aqueous medium using Lotus (Nelumbo nucifera) leaf powder chemically modified with dimethylamine: characterization, isotherms, kinetics, thermodynamics, and mechanism assessment, Int. J. Phytoremediat. 24 (2022) 131–144, https://doi.org/10.1080/15226514.2021.1929060.
[59] V. Belessi, G. Romanos, N. Boukos, D. Lambropoulou, C. Trapalis, Removal of Reactive Red 195 from aqueous solutions by adsorption on the surface of TiO_2 nanoparticles, J. Hazard. Mater. 170 (2009) 836–844, https://doi.org/10.1016/j.jhazmat.2009.05.045.
[60] M.Y. Nassar, I.S. Ahmed, T.Y. Mohamed, M. Khatab, A controlled, template-free, and hydrothermal synthesis route to sphere-like α-Fe_2O_3 nanostructures for textile dye removal, RSC Adv. 6 (2016) 20001–20013, https://doi.org/10.1039/c5ra26112k.
[61] H. Mahanna, M. Azab, Adsorption of Reactive Red 195 dye from industrial wastewater by dried soybean leaves modified with acetic acid, Desalin. Water Treat. 178 (2020) 312–321, https://doi.org/10.5004/dwt.2020.24960.
[62] G.K. Cheruiyot, W.C. Wanyonyi, J.J. Kiplimo, E.N. Maina, Adsorption of toxic crystal violet dye using coffee husks: Equilibrium, kinetics and thermodynamics study, Sci. African 5 (2019) 1–11, https://doi.org/10.1016/j.sciaf.2019.e00116.
[63] D.D. Eslek Koyuncu, M. Okur, Removal of AV 90 dye using ordered mesoporous carbon materials prepared via nanocasting of KIT-6: Adsorption isotherms, kinetics and thermodynamic analysis, Sep. Purif. Technol. 257 (2021) 117657.
[64] E.P. Fernandes, T.S. Silva, C.M. Carvalho, R. Selvasembian, N. Chaukura, L.M.T. M. Oliveira, S.M.P. Meneghetti, L. Meili, Efficient adsorption of dyes by γ-alumina synthesized from aluminum wastes: Kinetics, isotherms, thermodynamics and toxicity assessment, J. Environ. Chem. Eng. 9 (5) (2021) 106198.
[65] Y. Shang, Y. Cui, R. Shi, P. Yang, J. Wang, Y. Wang, Regenerated $WO_{2.72}$ nanowires with superb fast and selective adsorption for cationic dye: Kinetics, isotherm, thermodynamics, mechanism, J. Hazard. Mater. 379 (2019), https://doi.org/10.1016/j.jhazmat.2019.120834.
[66] N.A. Ahammad, M.A. Zulkifli, M.A. Ahmad, B.H. Hameed, A.T. Mohd Din, Desorption of chloramphenicol from ordered mesoporous carbon-alginate beads: Effects of operating parameters, and isotherm, kinetics, and regeneration studies, J. Environ Chem. Eng. 9 (1) (2021) 105015.